Published in final edited form as:
Bioconjug Chem. 2021 July 21; 32(7): 1276–1289. doi:10.1021/acs.bioconjchem.0c00401.

[^{68}Ga]Ga-THP-Pam: A Bisphosphonate PET Tracer with Facile Radiolabeling and Broad Calcium Mineral Affinity

George P. Keeling, **Billie Sherin**, **Jana Kim**, **Belinda San Juan**
School of Biomedical Engineering & Imaging Sciences, King's College London, London SEI 7EH, U.K

Tilmann Grus,
Department of Nuclear Chemistry, Johannes Gutenberg University Mainz, D-55128 Mainz, Germany

Thomas R. Eykyn,
School of Biomedical Engineering & Imaging Sciences, King's College London, London SEI 7EH, U.K

Frank Rösch,
Department of Nuclear Chemistry, Johannes Gutenberg University Mainz, D-55128 Mainz, Germany

Gareth E. Smith
Theragnostics Ltd, Bracknell, Berkshire RG12 1WA, U.K

Philip J. Blower, **Samantha Y. A. Terry**
School of Biomedical Engineering & Imaging Sciences, King's College London, London SE1 7EH, U.K

Rafael T. M. de Rosales[*]
School of Biomedical Engineering & Imaging Sciences, King's College London, London SEI 7EH, U.K

Abstract

Calcium minerals such as hydroxyapatite (HAp) can be detected noninvasively *in vivo* using nuclear imaging agents such as [^{18}F]NaF (available from cyclotrons), for positron emission tomography (PET) and ^{99m}Tc-radiolabeled bisphospho-nates (BP; available from ^{99m}Tc generators for single photon emission computed tomography (SPECT) or scintigraphy). These two types of imaging agents allow detection of bone metastases (based on the presence of HAp) and vascular calcification lesions (that contain HAp and other calcium minerals). With the aim of developing a cyclotron-independent PET radiotracer for these lesions, with broad calcium mineral affinity and simple one-step radiolabeling, we developed [^{68}Ga]Ga-THP-Pam. Radiolabeling with

[*]**Corresponding Author** rafael.torres@kcl.ac.uk.
Complete contact information is available at: https://pubs.acs.org/10.1021/acs.bioconjchem.0c00401

Notes
The authors declare the following competing financial interest(s): R.T.M.R. and P. J. B. are named inventors on related patents. All other authors have no conflicts to declare.

Europe PMC Funders Author Manuscripts

^{68}Ga is achieved using a mild single-step kit (5 min, room temperature, pH 7) to high radiochemical yield and purity (>95%). NMR studies demonstrate that Ga binds via the THP chelator, leaving the BP free to bind to its biological target. [^{68}Ga]Ga-THP-Pam shows high stability in human serum. The calcium mineral binding of [^{68}Ga]Ga-THP-Pam was compared *in vitro* to two other ^{68}Ga-BPs which have been successfully evaluated in humans, [^{68}Ga]Ga-NO2AP^{BP} and [^{68}Ga]Ga-BPAMD, as well as [^{18}F]NaF. Interestingly, we found that all ^{68}Ga-BPs have a high affinity for a broad range of calcium minerals implicated in vascular calcification disease, while [^{18}F]NaF is selective for HAp. Using healthy young mice as a model of metabolically active growing calcium mineral in vivo, we compared the pharmacokinetics and biodistribution of [^{68}Ga]Ga-THP-Pam with [^{18}F]NaF as well as [^{68}Ga]NO2AP^{BP}. These studies revealed that [^{68}Ga]Ga-THP-Pam has high in vivo affinity for bone tissue (high bone/muscle and bone/blood ratios) and fast blood clearance ($t_1/_2$ < 10 min) comparable to both [^{68}Ga]NO2AP^{BP} and [^{18}F]NaF. Overall, [^{68}Ga]Ga-THP-Pam shows high potential for clinical translation as a cyclotron-independent calcium mineral PET radiotracer, with simple and efficient radiochemistry that can be easily implemented in any radiopharmacy.

Introduction

Calcium is an essential element in human biology and the most abundant metallic element in the body by weight.[1,2] The majority of body calcium is in the form of a solid mineral, hydroxyapatite (HAp; $Ca_5(PO_4)_3(OH)$) in bones.[3] This calcium mineral can be targeted *in vivo* using bisphosphonates (BPs, Scheme 1A), which led to the development of BP-based radiotracers such as [^{99m}Tc]Tc-methylene diphosphonate (MDP) (^{99m}Tc; $t_{1/2}$ = 6.02 h). Introduced half a century ago, [^{99m}Tc]Tc-MDP is still widely used in nuclear medicine to image bone disease, particularly metastatic cancer in the bones using single photon emission computed tomography (SPECT) imaging (Scheme 1A).[4–7] Its chemical structure, however, remains unknown.[8]

In recent years there has been increasing interest in performing bone scans using positron emission tomography (PET) imaging. This is due to its better sensitivity and spatial resolution, compared to SPECT, which allows the detection of smaller lesions as well as improved image quantification. The radiotracer of choice in clinical PET imaging of bone lesions is the sodium salt of [^{18}F]fluoride (^{18}F; $t_{1/2}$ = 110 min; β^+ = 97%).[9–11] Interestingly, [^{18}F]NaF binds HAp not by interacting with calcium but by displacement of the hydroxide in the HAp lattice (Scheme 1A).[12]

Besides HAp, other calcium minerals are implicated in a number of health conditions in which a sensitive, noninvasive imaging method such as PET would be of great use. One such example is vascular calcification, a clinical marker of atherosclerosis in which soft vascular tissue forms plaques that can occlude the flow of blood through the affected vessel and can rupture, causing potentially fatal downstream effects.[13]

Atherosclerosis can lead to cardiovascular disease (CVD), the leading cause of death globally with *ca.* 18 million deaths in 2016 and an upward trend expected over the next decade.[14] The primary composition of vascular calcification lesions is disputed in the literature, with not only HAp but also calcium oxalate monohydrate and β-tricalcium

phosphate partially substituted with magnesium (whitlockite) being reported as the main components.[15–20] Other calcium minerals such as calcium carbonate, calcium pyrophosphate, and amorphous calcium phosphate have also been reported, as well as heterogeneous composition between patients.[15,18,21] Thus, it seems that calcium in these lesions is present as a mixture that may contain several non-HAp materials, summarized in Scheme 1B. The role that these non-HAp calcium minerals may have in different stages of CVD, and their potential as imaging biomarkers, remains to be elucidated.

Despite the advantages of [^{18}F]NaF as a PET radiotracer, its binding mechanism and *in vitro/vivo* data indicate that its target *in vivo* is HAp (Scheme 1A) and not other calcium minerals that have also been identified in vascular calcification lesions.[22,23] BPs on the other hand are not selective for HAp, showing broader calcium mineral affinity.[24,25] Hence, there is considerable interest in the development of BP-based PET radiotracers. These should allow the detection of bone lesions, as recently demonstrated in patients,[5,26–30] but also calcified vasculature which we have discussed above may contain different types of calcium minerals besides HAp and thus may benefit from the broader calcium mineral affinity of BPs.

From the radiopharmacy and clinical translation perspective, a disadvantage of current BP-based PET radiotracers is a relatively complex radiochemistry. ^{18}F is produced by cyclotrons, which are expensive and complex instruments but can produce [^{18}F]NaF in large quantities without any further need for complicated radiosynthetic procedures.[10] On the other hand, PET BPs rely on the use of radiometals and hence are bifunctional chelators that generally involve multistep syntheses and radiosynthetic procedures, which may require an automated synthesis module for clinical transla-tion.[5,26&28,31&40] The most promising radionuclide in the development of PET BPs is ^{68}Ga ($t_1/_2$ = 68 min; β^+ = 89%). This radiometal benefits from not only a short radiation decay half-life that minimizes radiation dose to patients but also availability from both cyclotrons and benchtop generators that can be installed in any radiopharmacy, allowing cyclotronindependent PET radiotracers on-site.[41] Having a variety of such cyclotron-independent radiotracers is attractive as it would not only provide an alternative supply of some PET radiotracers in the case of cyclotron failures but also potentially open the door to cyclotron-independent PET scanners, widening access to PET for patients geographically distant from cyclotron centers. Notable examples of ^{68}Ga radiotracers that are increasingly being exploited for clinical PET today include those based on PSMA for imaging prostate cancer,[42–44] octreotide analogues for neuroendocrine tu-mors,[45] and recently FAP inhibitors, which shows exciting prospects as a pan-cancer PET imaging agent.[46]

We set out to create a BP-based “cold kit” radio-pharmaceutical for PET imaging of calcium minerals, in which ^{68}Ga generator eluate could be added directly to a vial containing preformulated reagents and used without any further steps. Our motivation was not only to explore the broad calcium mineral affinity of BPs but also to combine the superior performance of PET imaging with the simplicity of radionuclide generator kit-based synthesis and availability, that has been largely responsible for the long-term success of ^{99m}Tc radiochemistry and the nuclear imaging field. Here, we describe the development of [^{68}Ga]Ga-THP-Pam, a ^{68}Ga complex of the efficient gallium chelator (tris)-

hydroxypyridinone (THP),[44,47–57] conjugated with the clinically used BP pamidronate (Pam) (Figure 1A) and its comparison with [^{18}F]NaF and two other ^{68}Ga-labeled BPs—BPAMD (Figure 1B) and NO2AP^{BP} (Figure 1C)—which have undergone extensive evaluation including first in human studies.[5,26&28,31&33,58]

Results and Discussion

Synthesis of THP-Pam

The bifunctional chelator THP-Pam was designed to include a (tris)hydroxypyridinone group for efficient gallium chelation, as well as the bone-targeting moiety pamidronate (Pam), a clinically used aminobisphosphonate with known high affinity for bone mineral.[59] Pamidronate was synthesized according to a literature procedure (Scheme 2A),[60] leading to a pure white solid with a shelf life at room temperature of at least 4485 days, as measured by NMR, MS, and elemental analysis. Among the clinically used second generation amino-BPs, pamidronate has the shorter chain between the BP and the amine groups, keeping the overall size of the molecule as small as possible, which generally leads to faster pharmacokinetics (PK).

In order to form the conjugate, the primary amine group of pamidronate was reacted with THP-isothiocyanate[50] in a single step (Scheme 2B). Water was chosen as the solvent for this reaction due to the poor solubility of amino-BPs in organic solvents.[24] This however opened the possibility of the slow degradation of the isothiocyanate in water. To increase the speed of reaction and reduce the likelihood of degradation, a minimal volume of solvent was used and the reaction was performed at 90 °C in a sealed vial with a large excess of pamidronate to help drive the desired reaction. Triethylamine was used to achieve a reaction pH of ~11 in order to deprotonate the amine of pamidronate (pK_a = 10.40-13.06)[61] and allow the reaction to proceed. The high pH increased the water solubility of both pamidronate and THP-NCS. Monitoring the progress of the reaction by LC/MS indicated that 2 h was the optimal reaction time. These reaction conditions were successful in reducing the number of byproducts; the only products observed by LC/MS, aside from excess pamidronate, were >90% THP-Pam (*m/z* $[M + 2H]^{2+}$ = 598) and <10% THP-NCS hydrolyzed to a primary amine (m/z $[M + 2H]^{2+}$ = 460).

The resulting thiourea bond has been reported to be less stable than amide bonds;[62,63] however, thiourea bonds have also been shown to be stable in vivo over time scales of up to 24 h.[64] Due to the short circulation time of BPs and short half-life of ^{68}Ga, the risk of hydrolysis of the thiourea bond during imaging was considered to be minimal. An amide bond formation would have been an alternative bioconjugation strategy, using N-hydroxysuccinimide esters. However, the relatively fast hydrolysis of the activated esters would have made water an unsuitable solvent for the required bioconjugation conditions (high pH and T) and the commercial availability of THP-isothiocyanate allowed for a more straightforward synthetic approach.

To remove the unreacted pamidronate, the reaction solution was loaded onto a Sep-Pak tC18 cartridge, from which pamidronate could selectively be eluted in water (0.1% TFA), while the other products were subsequently eluted in 1:1 water:acetonitrile (0.1% TFA). Collecting

small volume fractions, those with the most THP-Pam and least hydrolyzed THP-NCS, as measured using LC/MS, were collected. LC/MS analysis of the collated fractions confirmed the success of this purification step, with a final purity of >95% THP-Pam. After evaporation, THP-Pam was obtained as a white powder in 71% yield and no further attempts were made to optimize reaction conditions. The product can also be purified by semipreparative HPLC (HPLC method 1 (Table S1); t_R = 20.9 min).

Characterization of THP-Pam

Analytical C_{18} reversephase HPLC analysis showed a single peak (Figure 2A) with some tailing, indicating a pure product with multiple ionization states or different modes of retention on the stationary phase, as previously seen for other BP compounds.[24,31,32,38] THP-Pam eluted at t_R = 10.4 min (HPLC method 2 (Table S2)), at which point the mobile phase is ~70% water, as confirmed by LC/MS analysis (Figure 2B). Pamidronate, on the other hand, elutes at t_R = 1.7 min under the same conditions. After purification, LC/MS analyses occasionally indicated the presence of THP-Pam + Fe (m/z $[M + 2H]^{2+}$ = 625). This highlights the tendency for both THP and BPs to bind to metal ions, especially iron(III)[54,65&67] and the importance of avoiding metal contamination at any stage of reaction. Upon binding to iron, THP-Pam changes from a white powder to a pink or red powder, providing an extremely sensitive indicator of the presence of iron.[55] As this was not the case with our purified product, it was assumed that the iron was bound during transition through the LC/MS system and was not present in the product.

The $^{31}P\{^1H\}$ NMR spectrum of THP-Pam showed a single peak at 17.86 ppm, consistent with the chemical shift for a BP (Figure 2C). The ^1H NMR spectrum also showed the expected resonances for THP-Pam; however, all peaks were rather broad (Figure 2D). This is likely due to different ionization states of the molecule causing different conformations or small degrees of iron binding from solvent impurities. ^{19}F NMR revealed the presence of TFA salts in the final product (Figure 2E), even after low-vacuum evaporation. This was further confirmed by elemental analysis and is due to the presence of TFA in the mobile phases used during purification of THP-Pam.

As both pamidronate and THP are known metal chelators,[49,68] we conducted NMR studies in order to determine whether gallium will preferentially bind to THP, as expected due to its high affinity toward this metal, or if the BP could be involved. This is an important factor as competing of the BP with the chelator for the binding of gallium-68 has been noted in previous BP-based tracers.[32,36] To investigate this possibility, an aqueous solution (D_2O) of THP-Pam of known concentration and adjusted to pH 9 by addition of Na_2CO_3 was prepared at room temperature. To this solution, known amounts of nonradioactive gallium nitrate were added incrementally, and the binding process was monitored by $^{31}P\{^1H\}$ NMR to monitor the BP moiety, and the aromatic region of the ^1H NMR spectrum was monitored to monitor the hydroxypyridinone moieties responsible for the chelating properties of THP (Figure 3). As Ga(III) ions were added, a loss of symmetry and a change in chemical shift was observed in the aromatic region of the ^1H NMR spectrum (Figure 3A), indicating a change in the chemical environment of the hydroxypyridinone arms of THP and hence supportive of direct metal binding, as seen in previous THP studies.[69] Meanwhile the

bisphosphonate peak in the $^{31}P\{^{1}H\}$ NMR spectrum (Figure 3B) did not change, apart from minor peak broadening likely caused by slowing of the movement of the THP arms in response to metal binding and a minor chemical shift from 17.90 to 17.97 ppm as gallium was added. As a control, gallium nitrate was added to a solution of pamidronate under the same conditions and monitored by $^{31}P\{^{1}H\}$ NMR, and as expected, a distinct loss of symmetry and homogeneity was observed upon addition of gallium to the solution, with several new species with chemical shifts in the range of 22.4—3.0 ppm being formed (Figure 3C). Altogether, these data indicate that THP-Pam—at equimolar and subequimolar concentrations of gallium—will bind gallium in the THP chelator, and not the BP.

Radiochemistry

Having established that when reacting THP-Pam with gallium the metal ion binds to the THP chelator, and not the BP group, the radiolabeling reaction with ^{68}Ga was evaluated. It was found that ^{68}Ga radiolabeling is fast and efficient. In a typical reaction, a 250 μL aliquot of gallium-68 eluted from an Eckert and Ziegler $^{68}Ge/^{68}Ga$ generator in 0.1 M HCl was added to 4.18 nmol THP-Pam in water (5 μg) and neutralized with an aqueous 1 M solution of sodium bicarbonate. Both stock solutions were prepared using Chelex-treated water to minimize the presence of iron(III). After incubating the reaction for 5 min at room temperature, radio- ITLC and radio-HPLC indicated quantitative (>97%) complexation of ^{68}Ga (*vide infra*, Figure 4). We measured nonoptimized molar activities up to 17.3 MBq $nmol^{-1}$. In order to simplify this further to a preprepared kit, it is possible to freeze-dry the THP-Pam and sodium bicarbonate prior to reaction and elute the generator directly into a vial containing the dried reactants, scaling quantities as required. This opens up the possibility of GMP kit-based production of THP-Pam by simple addition of ^{68}Ga generator eluate into a sealed vial.

Radio-ITLC was performed using glass microfibre chromatography paper (ITLC) impregnated with silicic acid in order to retain [^{68}Ga]Ga-THP-Pam as well as possible. By developing the ITLC paper in 0.5 M citrate buffer, unbound ^{68}Ga moved with the solvent front, giving a clear distinction between [^{68}Ga]Ga-THP-Pam on the baseline (Figure 4A). This is in contrast to unbound ^{68}Ga, which primarily moves with the solvent front (Figure 4C). Radio-HPLC (C18-RP) was performed under the same conditions as analytical HPLC (method 2 (Table S2)). [^{68}Ga]Ga-THP-Pam eluted as a single peak with a retention time that is approximately 30 s later compared to THP-Pam, consistent with the expectation that the binding of the metal to the hydroxyl and ketone groups of THP leads to a small increase in lipophilicity and hence a slightly longer retention on reverse-phase HPLC (Figure 4B). Figure 4C-D shows the ITLC and radio-HPLC chromatograms of neutralized [^{68}Ga]$GaCl_3$ for comparison. Measurement of logP in water/octanol (-2.69 ± 0.03) and $logD_{7.4}$ in PBS/octanol (-2.72 ± 0.07) showed that [^{68}Ga]Ga-THP-Pam was highly hydrophilic as expected for a BP, as well as existing gallium-68 labeled conjugates of THP.[44]

The different radiochemical labeling conditions and purification steps required for the *in vivo* use of the different PET radiotracers discussed in this work (^{68}Ga-BPs and [^{18}F]NaF) have been outlined in Table 1. [^{18}F]NaF is received directly from the cyclotron and no radiochemistry is necessary, apart from two ion exchange cartridges prior to injection into

patients.[10] The radiolabeling processes of [^{68}Ga]Ga-BPAMD and [^{68}Ga]NO2AP^{BP} take advantage of the well-established radiochemistry associated with their chelators. In both cases, heating to 95 °C is required for radiolabeling.[31–32] Heating is a requirement for NO2AP^{BP} radiolabeling, despite the similarity between this chelator and NOTA, which can be labeled at room temperature.[70] In NO2AP^{BP}, however, the presence of the phosphonates allows the formation of an out-of-cage complex and so [^{68}Ga]Ga-NO2AP^{BP} cannot be prepared at room temperature.[32] The generator eluate may be processed prior to labeling of NO2AP^{BP} to allow milder heat to be used over a shorter time and to concentrate the eluate for greater molar activity;[71] however, this increases the number of steps during the radiolabeling process. Cooling and neutralization of the radiolabeling reactions are also required for [^{68}Ga]Ga-NO2AP^{BP} and [^{68}Ga]Ga-BPAMD. [^{68}Ga]Ga-BPAMD also requires purification postreaction.[31] THP-Pam on the other hand can be labeled in a single step at room temperature at neutral pH in 5 min. The THP chelator is selective for gallium(III) over other metals, and the labeling is not affected by metallic impurities at the levels found in typical ^{68}Ge/^{68}Ga generator elutions.[54,55] The efficient labeling of THP also allows for labeling at low concentrations and obviates the need for concentration of the generator eluate prior to labeling.[49]

In Vitro Stability

To evaluate the stability of [^{68}Ga]Ga- THP-Pam toward transchelation to plasma proteins, it was incubated in human serum at 37 °C for 3 h and the transchelation of ^{68}Ga was monitored by size-exclusion HPLC. This was monitored for 180 min, which was judged sufficient due to the short half-life of ^{68}Ga and fast pharmacokinetics commonly found with BPs (and hence imaging patients no later than 3 h postinjection). In this time frame, no transchelation of ^{68}Ga from [^{68}Ga]Ga-THP-Pam was observed and the complex remained intact and chemically unmodified. To further evaluate the stability of [^{68}Ga]Ga-THP-Pam, it was incubated in 1 mM EDTA solution in PBS (>1000-fold excess EDTA) at 37 °C for 3 h. After 3 h, the stability of [^{68}Ga]Ga-THP-Pam was 98.7 ± 1.2% (Figure S1). These results indicate not only the radiochemical stability of the [^{68}Ga]Ga-THP-Pam complex but also the stability of the thiourea bonds between the chelator and the BP under these conditions.

In comparison, Fellner et al. reported [^{68}Ga]Ga-BPAMD showed 4.2 ± 0.8% degradation over this time scale in PBS at 37 °C.[31] Serum stability has not been reported for [^{68}Ga]Ga-NO2AP^{BP}, but previous in vivo data for both small animals and humans demonstrated high stability for [^{68}Ga]Ga-BPAMD and [^{68}Ga]Ga-NO2AP^{BP}.[5,26–28–31–33] In support of this, the in vivo data reported here with [^{68}Ga]Ga-NO2AP^{BP} (*vide infra*) are in agreement with in vivo stability for this radiotracer.

In Vitro Calcium Mineral Binding

To assess the affinity and selectivity of different ^{68}Ga-BPs and [^{18}F]NaF toward several calcium minerals that are relevant to human disease, an in *vitro* binding assay was performed. The binding of [^{68}Ga]Ga- THP-Pam, [^{68}Ga]Ga-BPAMD, [^{68}Ga]Ga-NO2AP^{BP}, and [^{18}F]NaF to a range of calcium salts was compared, including blocking studies in which the calcium salts were preincubated with an excess of relevant blocking agents (nonradioactive fluoride or bisphosphonate) (Figure 5). All the tested agents showed high

binding to HAp (mean binding values in the range 78-93%) which could be blocked (mean values in the range 1-6%). [^{68}Ga]THP-Pam exhibited specific binding to all the tested salts, with the lowest value being the binding to calcium oxalate (mean value 31%). [^{68}Ga]Ga-NO2AP^{BP} generally exhibited the highest binding across the salts tested but with different trends to [^{68}Ga]Ga-THP-Pam, showing lower binding to calcium pyrophosphate (mean binding values of 45% vs 60%) but higher binding to calcium oxalate (mean binding 60%). [^{68}Ga]Ga-BPAMD generally showed the lowest binding of the ^{68}Ga-BPs, although it bound more to HAp than [^{68}Ga]Ga-THP-Pam (mean binding 87% vs 78%), but lower than [^{68}Ga]Ga-NO2AP^{BP} (mean binding 93%) and showed similar calcium pyrophosphate binding (mean binding 60%) to that of [^{68}Ga]Ga-THP-Pam. Contrary to expectation, the blocking experiments of [^{18}F]NaF with calcium carbonate, calcium phosphate, and calcium oxalate showed higher binding than the nonblocking experiments. The reason for this is unknown and may be due to the formation of an intermediate partially fluoridated salt due to the presence of higher concentrations of sodium fluoride in the blocking study, which can more readily bind [^{18}F]F^{-} than the original salt, although this hypothesis remains untested. Overall, it was found that ^{68}Ga-BPs and [^{18}F]NaF have high binding affinity toward HAp (mean binding of ^{68}Ga-BPs = 85.8 ± 4.3%, [^{18}F]NaF = 88.4 ± 4.6%), which could be blocked by using excess unlabeled BP or fluoride, respectively (mean blocked binding of ^{68}Ga-BPs = 2.6 ± 1.6%, [^{18}F]NaF = 2.2 ± 0.2%). For non-HAp calcium minerals, however, only ^{68}Ga-BPs showed significant binding (mean binding of ^{68}Ga-BPs across non-HAp minerals = 51.7 ± 18.0%) whereas binding of [^{18}F]NaF was negligible (mean binding of [^{18}F]NaF across non-HAp minerals = 8.4 ± 4.6%). Thus, these results are in agreement with the binding mechanisms outlined in Scheme 1, whereby BPs are able to bind to calcium ions on the surface of all these minerals. In the case of HAp, the only mineral with available hydroxyl groups within its lattice, [^{18}F]F^{-} substitution results in binding to the salt.[12] This confers HAp selectivity to [^{18}F]NaF. However, affinity to other calcium minerals may be advantageous in imaging ectopic or pathological calcification as previously discussed. In this regard, BP-based tracers may be of interest, in addition to their cyclotron-independent availability, in the imaging of vascular calcification in comparison to [^{18}F]NaF. The targeting of different calcium materials may also mean that combining ^{68}Ga-BPs and [^{18}F]NaF could provide complementary information which may be diagnostically useful in identifying non-HAp calcified deposits.

In Vivo Evaluation

To evaluate the *in vivo* pharmacokinetics (PK), biodistribution, and calcium mineral capabilities of these radiotracers, we compared [^{68}Ga]Ga-THP-Pam with [^{68}Ga]NO2AP^{BP} and [^{18}F]NaF in an *in vivo* PET imaging study in 6-8 week old healthy immunocompetent mice. This is a good model for the *in vivo* evaluation of calcium mineralseeking radiotracers as young mice have metabolically active growing bones. It is worth noting that [^{68}Ga]Ga-NO2AP^{BP} has previously been tested in patients, including a direct comparison to both [^{18}F]NaF and [^{99m}Tc]Tc-MDP.[5,28] Thus, it is a leading candidate for gallium-68 labeled BPs, and hence, it was chosen as a BP standard against which [^{68}Ga]Ga-THP-Pam could be compared. [^{18}F]NaF, due to the widespread use and its comparable results to [^{68}Ga]Ga-NO2AP^{BP} in patients with bone metastases,[5] was also included in our comparative *in vivo* study.

The *in vivo* PET-CT imaging results are shown in Figures 6 and 7. All radiotracers were injected intravenously and imaged dynamically for 60 min, showing fast PK profiles and high binding to bone, as expected. The main differences were related to kidney clearance and excretion. Both ^{68}Ga-BPs showed fast renal excretion, but [^{68}Ga]Ga-NO2AP^{BP} cleared faster from the kidneys than [^{68}Ga]Ga-THP-Pam, as demonstrated in Figure 7 by the visible kidney uptake at 40-59 min for [^{68}Ga]Ga-THP-Pam, which was barely visible after 20-40 min in the case of [^{68}Ga]Ga-NO2AP^{BP}. Interestingly, we found a lack of renal clearance with [^{18}F]NaF (Figure 6A). This was surprising as [^{18}F]NaF renal clearance/bladder accumulation is commonly observed in rodent studies, as well as in human clinical PET scans.[5,33] We believe this to be an experimental artifact due to the use of isoflurane anesthesia, but this hypothesis was not evaluated further. PK data were generated from regions of interest (ROI) within the PET images to calculate the fractions of injected dose per volume (mL) of tissue (Figure 6A). Using the knees as areas with known metabolically active new bone formation, the ROI image-analysis data showed a similar level of binding for both [^{68}Ga]Ga-THP-Pam (14.9 ± 1.0%ID mL^{-1} at 60 min) and [^{68}Ga]Ga-NO2AP^{BP} (15.7 ± 2.1%ID mL^{-1} at 60 min) (Figure 6B). Each plateaued at approximately 20 min postinjection. In the case of the animals injected with [^{18}F]NaF, knee uptake increased continuously 55 min postinjection, reaching 54.5 ± 5.1% ID mL^{-1} after 1 h. This significantly higher knee binding of fluoride vs BPs found may be attributable to the lack of excretion discussed above. To determine blood clearance, we used a ROI over the heart as a proxy and the data were fitted to a two-compartment PK model (Figure 6C). All radiotracers showed a two-stage blood clearance with a remarkably similar fast first half-life ($t_{1/2}$(fast) = 1.33 ± 0.12 min; mean ± SD for all three radiotracers), followed by a slower clearance stage ($t_{1/2}$(slow) < 12 min for all tracers), with the fastest being [^{68}Ga]Ga-NO2AP^{BP} ($t_{1/2}$(slow) = 6.6 min). Accordingly, the area under the curve from 3-59 min ($AUC_{3\text{-}59}$) for [^{68}Ga]Ga-NO2AP^{BP} (98.6 ± 3.4%ID min mL^{-1}) was lower than that of [^{68}Ga]Ga-THP-Pam (126.4 ± 7.5%ID min mL^{-1}), and [^{18}F]NaF (122.3 ± 5.1%ID min mL^{-1}). Thus, while both ^{68}Ga-BPs show comparable high bone uptake and fast PK profiles, [^{68}Ga]Ga-NO2AP^{BP} shows slightly faster circulation/renal clearance compared to [^{68}Ga]Ga-THP-Pam.

At the end of the imaging session mice were allowed to recover from anesthesia for 1 h to allow for further radiotracer clearance and subsequently culled for *ex vivo* biodistribution studies using gammain-counting (Figure 8; values are tabulated in Table S4). Despite the time lag of one hour, the in vivo PET imaging analyses results were in agreement with the ex vivo biodistribution, with [^{68}Ga]Ga-THP-Pam and [^{68}Ga]Ga-NO2AP^{BP} showing similarly high femur uptake values (14.1 ± 3.7%ID/g vs 20.1 ± 5.2% ID/g, respectively; $p = 0.101$) and [^{18}F]NaF having the highest of the three (47.1 ± 8.3% ID/g) (Figure 8). [^{68}Ga]Ga-THP-Pam showed higher accumulation in kidney and small intestines ($p < 0.001$), although these uptake values were very low (1.4-2.5% ID/g). These levels of kidney uptake are unlikely to interfere with the imaging of bone metastases or vascular calcification but may be problematic for imaging calcification in this organ. The bone-to-muscle ratios were similarly high (ca. 40) for all three radiotracers (Figure 8).

Conclusions

[^{68}Ga]Ga-THP-Pam, a new calcium-mineral targeted radiotracer, has been synthesized, characterized, and evaluated in *vitro* and in vivo. Using NMR studies, we demonstrate that gallium binds THP-Pam via the THP chelator and not the bisphosphonate moiety. The THP chelator allows high specific activity ^{68}Ga radiopharmaceuticals with high radiochemical purities (>95%) at room temperature and within minutes. These properties avoid the need for expensive/complicated instrumentation that is common in PET chemistry and allow simple and efficient kit-based radiosynthesis in any radiopharmacy. *In vitro* studies demonstrate that, in contrast to [^{18}F]NaF, which is selective to hydroxyapatite, ^{68}Ga-bi- sphosphonates have high binding affinity to several calcium salts that are present in human calcified vessels, including hydroxyapatite, with the binding of [^{68}Ga]Ga-THP-Pam generally found to be between those of [^{68}Ga]Ga-BPAMD and [^{68}Ga]Ga-NO2AP^{BP}. In vivo studies in healthy mice showed that both [^{68}Ga]Ga-THP-Pam and [^{68}Ga]Ga- NO2AP^{BP} (which has been successfully evaluated in humans, in comparison with [^{18}F]NaF) have a comparable high and rapid uptake in bone tissue, as well as fast blood clearance and urinary excretion. All these results highlight the potential of ^{68}Ga-bisphosphonates as cyclotron-independent alternatives to [^{18}F]NaF, as well as for the imaging of vascular calcification lesions. In addition, the fast, simple and efficient radio-chemistry required to synthesize [^{68}Ga]Ga-THP-Pam makes this radiotracer an appealing candidate for clinical translation.

Materials and Methods

Nomenclature of radiochemical species has been written in accordance with the conventions outlined by Coenen et al.[72]

Materials

THP-NCS was obtained from CheMatech, France. All other reagents were purchased from commercial sources unless stated otherwise. NO2AP^{BP} was synthesized according to ref 32. BPAMD was synthesized according to ref 58. Gallium-68 was eluted as [^{68}Ga]$GaCl_3$ from an Eckert and Ziegler ^{68}Ge/^{68}Ga generator in ultrapure HCl (5 mL, 0.1 M) manufactured to GMP requirements (ABX, Germany). [^{18}F]NaF in H_2O was purchased from Alliance Medical, U.K. ^{1}H and ^{31}P{^{1}H} NMR data were acquired on a Bruker 400 MHz and analyzed using MestReNova software. HPLC was performed on an Agilent 1260 Infinity instrument with UV spectroscopic detection at 254 nm and Lablogic Flow-Count detector with Bioscan Inc. B-FC-3200 photomultiplier tube detector and analyzed using Laura software. The mobile phase used for analytical and semipreparative reverse-phase HPLC was composed of A: water with 0.1% TFA and B: MeCN with 0.1% TFA. The mobile phase used for size-exclusion HPLC was PBS. LC/MS data were acquired on an Agilent 1200 Series Liquid Chromatograph with UV spectroscopic detection at 254 nm and same column details as in reverse-phase HPLC, interfaced with an Advion Expression^{L} CMS mass spectrometer with electrospray ionization source. The mobile phase used for LC/MS was composed of A: water with 0.1% formic acid; and B: MeCN with 0.1% formic acid. Cartridge purification was performed using Sep-Pak tC18 Long Cartridges with 900 mg sorbent per cartridge with a particle size of 37-55 μm. Radio instant thin layer

chromatography (ITLC) was developed on Agilent Technologies glass microfibre chromatography paper impregnated with silicic acid and analyzed using a Lablogic Flow-count TLC scanner and a BioScan B-FC-3200 PMT detector using Laura software. The ITLC mobile phase was composed of 0.175 M citric acid and 0.325 M trisodium citrate in water unless stated otherwise. Radioactive samples were measured using a Capintec CRC-25R or an LKB Wallac 1282 Compugamma CS for which data were collected using EdenTerm software. PET/CT images were acquired using a NanoPET/CT scanner (Mediso Ltd., Budapest, Hungary), reconstructed using Nucline v.0.21 software and images were analyzed using VivoQuant software (version 3.5, InviCRO Inc.). The centrifuge used was a Hettich MIKRO 20. Lyophilization was performed using an Edwards Freeze-Dryer Modulyo.

Synthesis of Disodium Pamidronate (Pam)

3-Amino-propionic acid (15 g, 0.168 mol) and phosphorous acid (20.7 g, 0.252 mol) were suspended in sulfolane (54 mL) and heated to 75 °C for 30 min. The mixture was allowed to cool to 35 °C and phosphorus trichloride (50 mL, 0.569 mol) was added gradually in aliquots. The solution was heated to 65 °C for 3 h with stirring and white precipitate began to form. The suspension was cooled to 0 °C and quenched by the slow addition of ice-cold water over 1 h to give a clear solution. The solution was heated to 100 °C for 3 h and then cooled to room temperature. Pamidronic acid was precipitated by the addition of ethanol, followed by filtration. The pamidronic acid was suspended in water (100 mL), and aqueous sodium hydroxide (20% w/w) was added with stirring until pH 8 was reached. The mixture was stirred at room temperature for 4 h. The solvents were evaporated, and the residue was recrystallized from water/ethanol to give pamidronate disodium dihydrate as a white powder (12.55 g, 39.8 mmol, 24%). ESI-MS: $[M + H]^+$ m/z = 235.0; calc. for $C_3H_{12}NO_7P_2$ = 235.0. ^1H NMR (D_2O, 400 MHz): δ 3.00-2.90 (2H, t), 2.00-1.88 (2H, m). ^{31}P NMR (D_2O, 162 MHz): δ 17.28. HPLC: 254 nm, t_R = 1.7 min, > 99% purity (HPLC method 2). Elemental analysis for disodium pamidronate + $2H_2O$: C = 11.84, H = 4.37, N = 4.45; calc.: C = 11.44, H = 4.16, N = 4.45.

Synthesis of THP-Pam

Pamidronate (14.5 mg, 52 μmol) was dissolved in a mixture of chelex-treated water (200 μL) and triethylamine (21.2 μL, 15.4 mg, 0.15 mmol) and heated to 90 °C. Separately, THP-NCS (5 mg, 5.2 μmol) was added to triethylamine (21.2 μL, 15.4 mg, 0.15 mmol) immediately followed by the addition of chelex-treated water (200 μL), and agitated to dissolve the THP-NCS. As soon as the THP-NCS had completely dissolved, the THP-NCS solution was added to the pamidronate solution and stirred in a sealed vial at 90 °C for 2 h. The crude mixture was loaded onto a prewashed Sep-Pak tC18 cartridge and the excess pamidronate was eluted in 5 mL water + 0.1% TFA. The product was eluted in 5 mL 50% water + 0.1% TFA/50% acetonitrile + 0.1% TFA and collected in 0.5 mL fractions. Fractions were analyzed by LCMS, and the relevant fractions were combined and lyophilized to yield a white powder (4.40 mg, 3.68 μmol, 71%). ESI-MS: $[M + 2H]^{2+}$ m/z = 598.7; calc. for $C_{48}H_{69}N_{11}O_{17}P_2S_2$ = 598.7. ^1H NMR (D_2O, 400 MHz): δ 7.30-7.05 (4H. m), 6.30-6.20 (3H, m), 4.48 (7H, s), 3.85—3.60 (6H, m), 3.49 (10H, m), 2.43-2.35 (4H, s), 2.23 (11H, m), 2.17-2.09 (8H, m),

1.95-1.82 (6H, m). ^{31}P NMR (D_2O, 162 MHz): δ 17.86. HPLC: 254 nm, t_R = 10.4 min, >99% purity (HPLC method 2).

NMR Studies of Gallium Binding

THP-Pam Gallium Binding—THP-Pam (2.25 mg, 1.88 umol) was dissolved in D_2O (600 uL), and sodium carbonate in D_2O (1 M) was added to keep the pH in the range 9 and increase solubility of THP-Pam. ^{1}H and ^{31}P NMR spectra were recorded. Gallium nitrate in D_2O (10 μL, 0.627 μmol, 62.7 mM) was added to the NMR tube, and more sodium carbonate was added to maintain a pH of 9 with shaking for 5 min. NMR spectra were recorded. This process was repeated two more times until 1 equiv of gallium had been added.

Pamidronate Gallium Binding—Pam (3.05 mg, 10.9 μmol) was dissolved in D_2O (600 μL), and sodium carbonate in D_2O (1 M) was added to keep the pH in the range 9 and increase solubility of THP-Pam. The ^{31}P NMR spectrum was recorded. Gallium nitrate in D_2O (43.67 μL, 2.75 μmol, 62.7 mM) was added to the NMR tube, and more sodium carbonate was added to maintain a pH of 9, with shaking for 5 min. The ^{31}P NMR spectrum was recorded. This process was repeated three more times until 1 equiv of gallium had been added.

Synthesis of [^{68}Ga]Ga-THP-Pam—A 1 mg mL^{-1} aqueous solution of THP-Pam in water was prepared. THP-Pam solution (5 μL, 5 μg, 4.18 nmol) was added to [^{68}Ga]$GaCl_3$ (250 μL, 15-90 MBq). Sodium bicarbonate solution in water (26 μL, 1 M) was added immediately. The mixture was agitated and the pH was checked to ensure it was in the range 6.5-7.5. Radiochemical yield and purity were evaluated after 5 min by ITLC (unbound ^{68}Ga Rf = 0.8-1; [^{68}Ga]Ga-THP-Pam Rf = 0-0.3) and after 10 min by HPLC, method 2 (unbound ^{68}Ga t_R = 1.9 min; [^{68}Ga]Ga-THP-Pam t_R = 10.8 min).

Synthesis of [^{68}Ga]Ga-NO2AP^{BP} —Gallum-68 (140-200 MBq) eluted from a generator was passed through a Phenomenex Strata-X-C 33 μm SPE cartridge. The cartridge was washed with acetone/0.1 M hydrochloric acid (80:20 v/v, 5 mL) to remove trace metal impurities. The gallium-68 was recovered from the cartridge by washing slowly with acetone/ 0.05 M hydrochloric acid (98/2 v/v, 700 μL) and added to aqueous HEPES buffer (pH 4, 0.125 M, 400 μL). Aqueous 1 mg mL^{-1} NO2AP^{BP} (8.69 μL, 8.69 μg, 17 nmol) was added to the gallium-68/HEPES solution followed by heating to 95 °C for 10 min with venting to allow the acetone to evaporate. After cooling, pH was adjusted to 7 by adding aqueous sodium hydroxide (~10 μL, 1 M).

Determination of LogP and Log D_{74} Values—For logP measurement, aliquots of [^{68}Ga]Ga-THP-Pam (10 μL, ~ 700 kBq) were added to vials containing a mixture of octanol presaturated with water (500 μL) and water presaturated with octanol (500 μL). The tubes were shaken for 3 min, and the mixture was centrifuged for 5 min to separate the octanol and PBS phases. Aliquots (50 μL) of each phase were taken and transferred to separate vials for counting of radioactivity. For measurement of log$D_{7.4}$ the same procedure was performed, using PBS in place of water.

Serum Stability—Freshly filtered human serum (200 μL) was added to a tube containing normal saline (100 μL) followed by incubation at 37 °C. [^{68}Ga]Ga-THP-Pam (100 μL, ~7 MBq) was added. Size exclusion HPLC (using method 3 (Table S3) was run prior to incubation and after 60 and 180 min of incubation. Serum proteins eluted at 5.0-9.0 min. [^{68}Ga]Ga-THP-Pam eluted at 11.0 min.

Stability to EDTA Competition—An aliquot of EDTA solution in PBS (950 μL, 1 mM) was incubated at 37 °C. [^{68}Ga]Ga-THP-Pam (50 μL, ~20 MBq) was added to the EDTA solution and incubated with stirring. Samples were analyzed by ITLC (mobile phase: 1 M ammonium acetate in 1:1 water/methanol) after 60 and 180 min. Controls were performed using [^{68}Ga]$GaCl_3$ neutralized according to the method used in the synthesis of [^{68}Ga]Ga-THP-Pam, in the absence of the THP-Pam ligand. Unbound ^{68}Ga R_f = 0-0.3; [^{68}Ga]Ga-THP-Pam R_f = 0-0.3; [^{68}Ga]Ga-EDTA R_f = 0.7-1.

Binding to Calcium Salts—A suspension of HAp (1 mg) in saline (1 mL) was prepared. For the blocking study this was prepared in advance with pamidronate (27.9 mg, 100 μmol) and incubated overnight prior to reaction. Once the suspensions were prepared, an aliquot of the reaction mixture containing the radiotracer (10 μL, ~700 kBq) was added to the suspension and incubated at room temperature for 1 h with continuous shaking. The suspensions were centrifuged at 9677 g for 5 min, and the supernatant was removed to a new tube and the activities of both fractions were measured. All the above steps were also repeated with other calcium salts (CC, CP dibasic, CPy, β-TCP, CO). These measurements were repeated for [^{68}Ga]Ga-BPAMD (blocking with alendronate), [^{68}Ga]Ga-NO2AP^{BP} (blocking with pamidronate), and [^{18}F]NaF (blocking with sodium fluoride).

PET-CT Imaging—Animal imaging studies were ethically reviewed and carried out in accordance with the Animals (Scientific Procedures) Act 1986 (ASPA) U.K. Home Office regulations governing animal experimentation. Each mouse (5 per tracer, of which 4 were imaged and 1 was used only for biodistribution studies, normal BALB/c, female, aged 6-8 weeks, 17-20 g body weight) was anaesthetized by inhalation of isoflurane (2-3% in oxygen), and the tail vein was cannulated. Then the mouse was placed in a preclinical PET/CT scanner, where anesthesia was maintained and the bed was heated to maintain normal body temperature. CT was performed followed by 1 h PET acquisition (1:5 coincidence mode; 5 ns coincidence time window). After the first minute, the radiopharmaceutical (100 ± 15 μL, 2.2-16.2 MBq) was injected and the animal was scanned. At the end of the scan, the animal was removed and allowed to recover for a further hour and culled at 2 h postinjection for biodistribution studies. Organs were harvested, weighed, and counted with a gamma counter along with standards prepared from injected material. Dynamic PET/CT images were reconstructed using Tera- Tomo 3D reconstruction (400-600 keV energy window, 1-3 coincidence mode, 4 iterations and subsets) at a voxel size of (0.4 × 0.4 × 0.4) mm^3 and corrected for attenuation, scatter and decay. The data were binned into 17 frames (1 × 1, 10 × 3, 5 × 5 and 1 × 4 min) for dynamic analysis. Regions of interest were drawn over the knees as an area of growing bone, heart as an indication of blood, kidneys, bladder, and liver.

Acknowledgments

The authors would like to thank A. Mishra, A. Khan, J. Jackson, and P. Gawne for their assistance during the *in vivo* work and D. Thakor, M. Hutchings, K. Sunassee, and S. Catchpole for their technical support. Elemental analyses were performed by Stephen Young, Chief Research Technician, Microanalysis, Department of Chemistry, University of Cambridge. This work was funded by the EPSRC Centre for Doctoral Training in Medical Imaging [EP/L015226/1], Theragnostics Ltd., the Wellcome/EPSRC Centre for Medical Engineering [WT/ 203148/Z/16/Z], and the EPSRC programme for next generation molecular imaging and therapy with radionuclides [EP/S032789/1]. Further support comes from a Wellcome Trust Multi User Equipment Grant: A multiuser radio-analytical facility for molecular imaging and radionuclide therapy research and the National Institute for Health Research (NIHR) Biomedical Research Centre based at Guy's and St Thomas' NHS Foundation Trust and KCL [grant number IS-BRC-1215-20006]. PET and SPECT scanning equipment at KCL was funded by an equipment grant from the Wellcome Trust under grant number WT 084052/Z/07/Z. The views expressed are those of the authors and not necessarily those of the NHS, the NIHR, or the Department of Health.

References

(1). Peacock M. Calcium Metabolism in Health and Disease. Clin J Am Soc Nephrol. 2010; 5:S23–S30. [PubMed: 20089499]

(2). Lippard, SJ, Berg, JM. Principles of bioinorganic chemistry. University Science Books; Mill Valley, CA: 1994.

(3). Clarke B. Normal bone anatomy and physiology. Clin J Am Soc Nephrol. 2008; 3:S131–S139. [PubMed: 18988698]

(4). O'Sullivan GJ, Carty FL, Cronin CG. Imaging of bone metastasis: An update. World J Radiol. 2015; 7:202–211. [PubMed: 26339464]

(5). Pfannkuchen N, Meckel M, Bergmann R, Bachmann M, Bal C, Sathekge M, Mohnike W, Baum R, Rösch F. Novel Radiolabeled Bisphosphonates for PET Diagnosis and Endoradiotherapy of Bone Metastases. Pharmaceuticals. 2017; 10:45.

(6). Qiu L, Lin JG, Ju XH, Gong XD, Luo SN. Structural Investigation of Technetium-Diphosphonate Complex Tc-99m-MDP. Chin J Chem Phys. 2011; 24:295–304.

(7). Subramanian G, McAfee JG, Blair RJ, Kallfelz FA, Thomas FD. Technetium 99m methylene diphosphonate: a superior agent for skeletal imaging: Comparison with other technetium complexes. J Nucl Med. 1975; 16:744–755. [PubMed: 170385]

(8). Handeland A, Lindegaard MW, Heggli DE. Biodistribution of anionic separated MDP complexes from different MDP preparations. Eur J Nucl Med. 1989; 15:609–611. [PubMed: 2598957]

(9). Hillner BE, Siegel BA, Hanna L, Duan F, Quinn B, Shields AF. 18F-Fluoride PET Used for Treatment Monitoring of Systemic Cancer Therapy: Results from the National Oncologic PET Registry. J Nucl Med. 2015; 56:222–228. [PubMed: 25593113]

(10). Beheshti M, Mottaghy FM, Payche F, Behrendt FFF, Van den Wyngaert T, Fogelman I, Strobel K, Celli M, Fanti S, Giammarile F, et al. 18F-NaF PET/CT: EANM procedure guidelines for bone imaging. Eur J Nucl Med Mol Imaging. 2015; 42:1767–1777. [PubMed: 26201825]

(11). Segall G, Delbeke D, Stabin MG, Even-Sapir E, Fair J, Sajdak R, Smith GT. SNM Practice Guideline for Sodium 18F-Fluoride PET/CT Bone Scans 1.0. J Nucl Med. 2010; 51:1813–1820. [PubMed: 21051652]

(12). Czernin J, Satyamurthy N, Schiepers C. Molecular Mechanisms of Bone 18F-NaF Deposition. J Nucl Med. 2010; 51:1826–1829. [PubMed: 21078790]

(13). Doherty TM, Asotra K, Fitzpatrick LA, Qiao J-H, Wilkin DJ, Detrano RC, Dunstan CR, Shah PK, Rajavashisth TB. Calcification in atherosclerosis: Bone biology and chronic inflammation at the arterial crossroads. Proc Natl Acad Sci U S A. 2003; 100:11201–11206. [PubMed: 14500910]

(14). Virani SS, Alonso A, Benjamin EJ, Bittencourt MS, Callaway CW, Carson AP, Chamberlain AM, Chang AR, Cheng S, Delling FN, et al. Heart Disease and Stroke Statistics-2020 Update: A Report From the American Heart Association. Circulation. 2020; 141:e139–e596. [PubMed: 31992061]

(15). Nishizawa Y, Higuchi C, Nakaoka T, Omori H, Ogawa T, Sakura H, Nitta K. Compositional Analysis of Coronary Artery Calcification in Dialysis Patients in vivo by Dual-Energy Computed Tomography Angiography. Ther Apheresis Dial. 2018; 22:365–370.

(16). Schwarz U, Buzello M, Ritz E, Stein G, Raabe G, Wiest G, Mall G, Amann K. Morphology of coronary atherosclerotic lesions in patients with end-stage renal failure. Nephrol Dial Transplant. 2000; 15:218–23. [PubMed: 10648668]

(17). Schlieper G, Aretz A, Verberckmoes SC, Krüger T, Behets GJ, Ghadimi R, Weirich TE, Rohrmann D, Langer S, Tordoir JH, et al. Ultrastructural analysis of vascular calcifications in uremia. J Am Soc Nephrol. 2010; 21:689–696. [PubMed: 20203159]

(18). O'Neill WC. Vascular calcification: Not so crystal clear. Kidney Int. 2007; 71:282–283. [PubMed: 17287816]

(19). Villa-Bellosta R, Egido J. Phosphate, pyrophosphate, and vascular calcification: a question of balance. Eur Heart J. 2015; 38:1801–1804.

(20). Reid JD, Andersen ME. Medial calcification (whitlockite) in the aorta. Atherosclerosis. 1993; 101:213–24. [PubMed: 8379966]

(21). Lee JS, Morrisett JD, Tung C-H. Detection of hydroxyapatite in calcified cardiovascular tissues. Atherosclerosis. 2012; 224:340–347. [PubMed: 22877867]

(22). Creager MD, Hohl T, Hutcheson JD, Moss AJ, Schlotter F, Blaser MC, Park M-A, Lee LH, Singh SA, Alcaide-Corral CJ, et al. 18F-Fluoride Signal Amplification Identifies Microcalcifications Associated With Atherosclerotic Plaque Instability in Positron Emission Tomography/Computed Tomography Images. Circ Cardiovasc Imaging. 2019; 12 e007835 [PubMed: 30642216]

(23). Irkle A, Vesey AT, Lewis DY, Skepper JN, Bird JLE, Dweck MR, Joshi FR, Gallagher FA, Warburton EA, Bennett MR, et al. Identifying active vascular microcalcification by F-18-sodium fluoride positron emission tomography. Nat Commun. 2015; 6:11.

(24). de Rosales RTM, Finucane C, Mather SJ, Blower PJ. Bifunctional bisphosphonate complexes for the diagnosis and therapy of bone metastases. Chem Commun. 2009:4847–4849.

(25). de Rosales RTM, Tavare R, Paul RL, Jauregui-Osoro M, Protti A, Glaria A, Varma G, Szanda I, Blower PJ. Synthesis of Cu-64(II)-Bis(dithiocarbamatebisphosphonate) and Its Conjugation with Superparamagnetic Iron Oxide Nanoparticles: In Vivo Evaluation as Dual-Modality PET-MRI Agent. Angew Chem Int Ed. 2011; 50:5509–5513.

(26). Fellner M, Baum RP, Kubicek V, Hermann P, Lukes I, Prasad V, Rosch F. PET/CT imaging of osteoblastic bone metastases with Ga-68-bisphosphonates: first human study. Eur J Nucl Med Mol Imaging. 2010; 37:834–834. [PubMed: 20069291]

(27). Khawar A, Eppard E, Roesch F, Ahmadzadehfar H, Kurpig S, Meisenheimer M, Gaertner FC, Essler M, Bundschuh RA. Preliminary results of biodistribution and dosimetric analysis of Ga-68 Ga-DOTA(ZOL): a new zoledronate-based bisphosphonate for PET/CT diagnosis of bone diseases. Ann Nucl Med. 2019; 33:404–413. [PubMed: 30877560]

(28). Passah A, Tripathi M, Ballal S, Yadav MP, Kumar R, Roesch F, Meckel M, Sarathi Chakraborty P, Bal C. Evaluation of bone-seeking novel radiotracer 68Ga-NO2AP-Bisphosphonate for the detection of skeletal metastases in carcinoma breast. Eur J Nucl Med Mol Imaging. 2017; 44:41–49.

(29). Doot RK, Young AJ, Daube-Witherspoon ME, Alexoff D, Labban KJ, Lee H, Wu Z, Zha Z, Choi SR, Ploessl KH, et al. Biodistribution, dosimetry, and temporal signal-to-noise ratio analyses of normal and cancer uptake of [68Ga]Ga-P15-041, a gallium-68 labeled bisphosphonate, from first-in-human studies. Nucl Med Biol. 2020; 86-87:1–8. [PubMed: 32361089]

(30). Lawal IO, Mokoala KMG, Mahapane J, Kleyhans J, Meckel M, Vorster M, Ebenhan T, Rosch F, Sathekge MM. A prospective intra-individual comparison of Ga-68 Ga-PSMA-11 PET/CT, Ga-68 Ga-NODAGA(ZOL) PET/CT, and Tc-99m Tc-MDP bone scintigraphy for radionuclide imaging of prostate cancer skeletal metastases. Eur J Nucl Med Mol Imaging. 2020; doi: 10.1007/s00259-020-04867-y

(31). Fellner M, Biesalski B, Bausbacher N, Kubicek V, Hermann P, Rosch F, Thews O. Ga-68-BPAMD: PET-imaging of bone metastases with a generator based positron emitter. Nucl Med Biol. 2012; 39:993–999. [PubMed: 22633217]

(32). Holub J, Meckel M, Kubicek V, Rosch F, Hermann P. Gallium(III) complexes of NOTA-bis (phosphonate) conjugates as PET radiotracers for bone imaging. Contrast Media Mol Imaging. 2015; 10:122–34. [PubMed: 24801892]

(33). Meckel M, Fellner M, Thieme N, Bergmann R, Kubicek V, Rosch F. In vivo comparison of DOTA based Ga-68-labelled bisphosphonates for bone imaging in non-tumour models. Nucl Med Biol. 2013; 40:823–830. [PubMed: 23915801]

(34). Rosch F, Baum RP. Generator-based PET radiopharmaceuticals for molecular imaging of tumours: on the way to THERANOSTICS. Dalton Trans. 2011; 40:6104–11. [PubMed: 21445433]

(35). Suzuki K, Satake M, Suwada J, Oshikiri S, Ashino H, Dozono H, Hino A, Kasahara H, Minamizawa T. Synthesis and evaluation of a novel Ga-68-chelate-conjugated bisphosphonate as a bone-seeking agent for PET imaging. Nucl Med Biol. 2011; 38:1011–1018. [PubMed: 21982572]

(36). Notni J, Plutnar J, Wester HJ. Bone-seeking TRAP conjugates: surprising observations and their implications on the development of gallium-68-labeled bisphosphonates. EJNMMI Res. 2012; 2:2. [PubMed: 22264389]

(37). Wu Z, Zha Z, Choi SR, Plossl K, Zhu L, Kung HF. New (68)Ga-PhenA bisphosphonates as potential bone imaging agents. Nucl Med Biol. 2016; 43:360–71. [PubMed: 27260777]

(38). Meckel M, Bergmann R, Miederer M, Roesch F. Bone targeting compounds for radiotherapy and imaging: *Me(III)-DOTA conjugates of bisphosphonic acid, pamidronic acid and zoledronic acid. EJNMMI Radiopharm Chem. 2017; 1:14. [PubMed: 29564390]

(39). Ahrens BJ, Li L, Ciminera AK, Chea J, Poku E, Bading JR, Weist MR, Miller MM, Colcher DM, Shively JE. Diagnostic PET Imaging of Mammary Microcalcifications Using Cu-64-DOTA-Alendronate in a Rat Model of Breast Cancer. J Nucl Med. 2017; 58:1373–1379. [PubMed: 28450564]

(40). Zha Z, Wu Z, Choi SR, Ploessl K, Smith M, Alexoff D, Zhu L, Kung HF. A New [68Ga]Ga-HBED-CC-Bisphosphonate as a Bone Imaging Agent. Mol Pharmaceutics. 2020; 17:1674–1684.

(41). Fani M, Andre JP, Maecke HR. 68Ga-PET: a powerful generator-based alternative to cyclotron-based PET radiopharmaceuticals. Contrast Media Mol Imaging. 2008; 3:53–63. [PubMed: 18383455]

(42). Banerjee SR, Pullambhatla M, Byun Y, Nimmagadda S, Green G, Fox JJ, Horti A, Mease RC, Pomper MG. 68Ga-Labeled Inhibitors of Prostate-Specific Membrane Antigen (PSMA) for Imaging Prostate Cancer. J Med Chem. 2010; 53:5333–5341. [PubMed: 20568777]

(43). Eder M, Schäfer M, Bauder-Wüst U, Hull W-E, Wängler C, Mier W, Haberkorn U, Eisenhut M. 68Ga-Complex Lipophilicity and the Targeting Property of a Urea-Based PSMA Inhibitor for PET Imaging. Bioconjugate Chem. 2012; 23:688–697.

(44). Young JD, Abbate V, Imberti C, Meszaros LK, Ma MT, Terry SYA, Hider RC, Mullen GE, Blower PJ. Ga-68-THP-PSMA: A PET Imaging Agent for Prostate Cancer Offering Rapid, Room-Temperature, 1-Step Kit-Based Radiolabeling. J Nucl Med. 2017; 58:1270–1277. [PubMed: 28408532]

(45). Graham MM, Gu X, Ginader T, Breheny P, Sunderland J. 68Ga-DOTATOC Imaging of Neuroendocrine Tumors: A Systematic Review and Meta-Analysis. J Nucl Med. 2017; 58:1452. [PubMed: 28280220]

(46). Giesel FL, Kratochwil C, Lindner T, Marschalek MM, Loktev A, Lehnert W, Debus J, Jager D, Flechsig P, Altmann A, et al. Ga-68-FAPI PET/CT: Biodistribution and Preliminary Dosimetry Estimate of 2 DOTA-Containing FAP-Targeting Agents in Patients with Various Cancers. J Nucl Med. 2019; 60:386–392. [PubMed: 30072500]

(47). Ma MT, Cullinane C, Waldeck K, Roselt P, Hicks RJ, Blower PJ. Rapid kit-based (68)Ga-labelling and PET imaging with THP-Tyr(3)-octreotate: a preliminary comparison with DOTA-Tyr(3)-octreotate. EJNMMI Res. 2015; 5:52. [PubMed: 26452495]

(48). Hofman MS, Eu P, Jackson P, Hong E, Binns D, Iravani A, Murphy D, Mitchell C, Siva S, Hicks RJ, et al. Cold Kit for Prostate-Specific Membrane Antigen (PSMA) PET Imaging: Phase 1 Study of (68)Ga-Tris(Hydroxypyridinone)-PSMA PET/CT in Patients with Prostate Cancer. J Nucl Med. 2018; 59:625–631. [PubMed: 28986512]

(49). Berry DJ, Ma YM, Ballinger JR, Tavare R, Koers A, Sunassee K, Zhou T, Nawaz S, Mullen GED, Hider RC, et al. Efficient bifunctional gallium-68 chelators for positron emission tomography: tris(hydroxypyridinone) ligands. Chem Commun. 2011; 47:7068–7070.

(50). Ma MT, Cullinane C, Imberti C, Baguna Torres J, Terry SYA, Roselt P, Hicks RJ, Blower PJ. New Tris(hydroxypyridinone) Bifunctional Chelators Containing Isothiocyanate Groups Provide a Versatile Platform for Rapid One Step Labeling and PET Imaging with Ga-68(3+). Bioconjugate Chem. 2016; 27:309–318.

(51). Imberti C, Terry SYA, Cullinane C, Clarke F, Cornish GH, Ramakrishnan NK, Roselt P, Cope AP, Hicks RJ, Blower PJ, et al. Enhancing PET Signal at Target Tissue in Vivo: Dendritic and Multimeric Tris(hydroxypyridinone) Conjugates for Molecular Imaging of alpha(v)beta(3) Integrin Expression with Gallium-68. Bioconjugate Chem. 2017; 28:481–495.

(52). Nawaz S, Mullen GED, Sunassee K, Bordoloi J, Blower PJ, Ballinger JR. Simple, mild, one-step labelling of proteins with gallium-68 using a tris(hydroxypyridinone) bifunctional chelator: a 68Ga-THP-scFv targeting the prostate-specific membrane antigen. EJNMMI Res. 2017; 7:86. [PubMed: 29067565]

(53). Tsionou MI, Knapp CE, Foley CA, Munteanu CR, Cakebread A, Imberti C, Eykyn TR, Young JD, Paterson BM, Blower PJ, et al. Comparison of macrocyclic and acyclic chelators for gallium-68 radiolabelling. RSC Adv. 2017; 7:49586–49599. [PubMed: 29308192]

(54). Cusnir R, Cakebread A, Cooper MS, Young JD, Blower PJ, Ma MT. The effects of trace metal impurities on Ga-68-radiolabelling with a tris(3-hydroxy-1,6-dimethylpyridin-4-one) (THP) chelator. RSC Adv. 2019; 9:37214–37221.

(55). Imberti C, Chen YL, Foley CA, Ma MT, Paterson BM, Wang YF, Young JD, Hider RC, Blower PJ. Tuning the properties of tris(hydroxypyridinone) ligands: efficient Ga-68 chelators for PET imaging. Dalton Trans. 2019; 48:4299–4313. [PubMed: 30860215]

(56). Imberti C, Adumeau P, Blower JE, Al Salemee F, Torres JB, Lewis JS, Zeglis BM, Terry SYA, Blower PJ. Manipulating the In Vivo Behaviour of Ga-68 with Tris- (Hydroxypyridinone) Chelators: Pretargeting and Blood Clearance. Int J Mol Sci. 2020; 21:1496.

(57). Cusnir R, Imberti C, Hider RC, Blower PJ, Ma MT. Hydroxypyridinone Chelators: From Iron Scavenging to Radiopharmaceuticals for PET Imaging with Gallium-68. Int J Mol Sci. 2017; 18:116.

(58). Kubicek V, Rudovsky J, Kotek J, Hermann P, Elst LV, Muller RN, Kolar ZI, Wolterbeek HT, Peters JA, Lukes I. A bisphosphonate monoamide analogue of DOTA: A potential agent for bone targeting. J Am Chem Soc. 2005; 127:16477–16485. [PubMed: 16305234]

(59). Fitton A, McTavish D. Pamidronate. A review of its pharmacological properties and therapeutic efficacy in resorptive bone disease. Drugs. 1991; 41:289–318. [PubMed: 1709854]

(60). Patel VM, Chitturi TR, Thennati R. Google Patents. 2008 US7411087B2

(61). Alanne A-L, Hyvonen H, Lahtinen M, Ylisirnio M, Turhanen P, Kolehmainen E, Peraniemi S, Vepsalainen J. Systematic study of the physicochemical properties of a homologous series of aminobisphosphonates. Molecules. 2012; 17:10928–10945. [PubMed: 22971579]

(62). Algar, WR. A Brief Introduction to Traditional Bioconjugate ChemistryChemoselective and Bioorthogonal Ligation Reactions: Concepts and Application. Algar, WR, Dawson, PE, Medintz, IL, editors. Wiley-VCH; Weinheim, Germany: 2018. 3–36.

(63). Banks PR, Paquette DM. Comparison of Three Common Amine Reactive Fluorescent Probes Used for Conjugation to Biomolecules by Capillary Zone Electrophoresis. Bioconjugate Chem. 1995; 6:447–458.

(64). Landel AM. Stability studies on fluorescein isothiocyanate-bovine serum albumin conjugate. Anal Biochem. 1976; 73:280–289. [PubMed: 962043]

(65). Fleisch H. Bisphosphonates: Mechanisms of Action. Endocr Rev. 1998; 19:80–100. [PubMed: 9494781]

(66). de Rosales TMR, Tavare R, Glaria A, Varma G, Protti A, Blower PJ. Tc-99m-Bisphosphonate-Iron Oxide Nanoparticle Conjugates for Dual-Modality Biomedical Imaging. Bioconjugate Chem. 2011; 22:455–465.

(67). Sandiford L, Phinikaridou A, Protti A, Meszaros LK, Cui XJ, Yan Y, Frodsham G, Williamson PA, Gaddum N, Botnar RM, et al. Bisphosphonate-Anchored PEGylation and Radiolabeling of Superparamagnetic Iron Oxide: Long-Circulating Nanoparticles for in Vivo Multimodal (T1MRI-SPECT) Imaging. ACS Nano. 2013; 7:500–512. [PubMed: 23194247]

(68). Subramanian G, McAfee JG. A new complex of 99mTc for skeletal imaging. Radiology. 1971; 99:192–6. [PubMed: 5548678]

(69). Young, J. Imaging and Therapeutic Radiotracers for Prostate Cancer. Ph.D. Thesis, King's College London; London, U.K: 2018.

(70). Velikyan I, Maecke H, Langstrom B. Convenient Preparation of 68Ga-Based PET-Radiopharmaceuticals at Room Temperature. Bioconjugate Chem. 2008; 19:569–573.

(71). Seemann J, Eppard E, Waldron BP, Ross TL, Roesch F. Cation exchange-based post-processing of Ga-68-eluate: A comparison of three solvent systems for labelling of DOTATOC, NO2AP(BP) and DATA(m). Appl Radiat Isot. 2015; 98:54–59. [PubMed: 25638573]

(72). Coenen HH, Gee AD, Adam M, Antoni G, Cutler CS, Fujibayashi Y, Jeong JM, Mach RH, Mindt TL, Pike VW, et al. Consensus nomenclature rules for radiopharmaceutical chemistry — Setting the record straight. Nucl Med Biol. 2017; 55

Europe PMC Funders Author Manuscripts

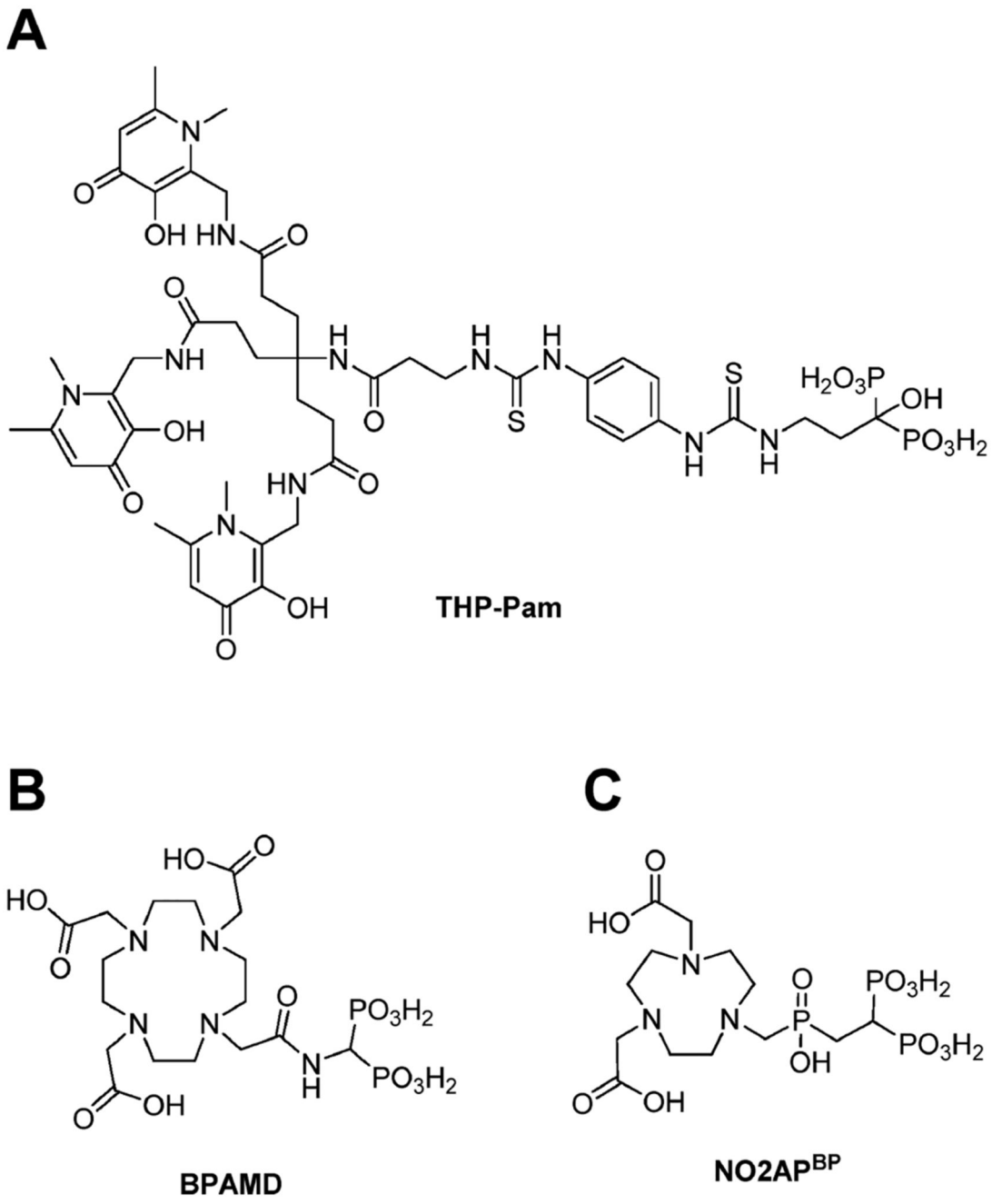

Figure 1. Chemical structures of the bifunctional bisphosphonate chelators discussed in this work: (A) THP-Pam; (B) BPAMD; (C) NO2AP^{bp}.

Europe PMC Funders Author Manuscripts

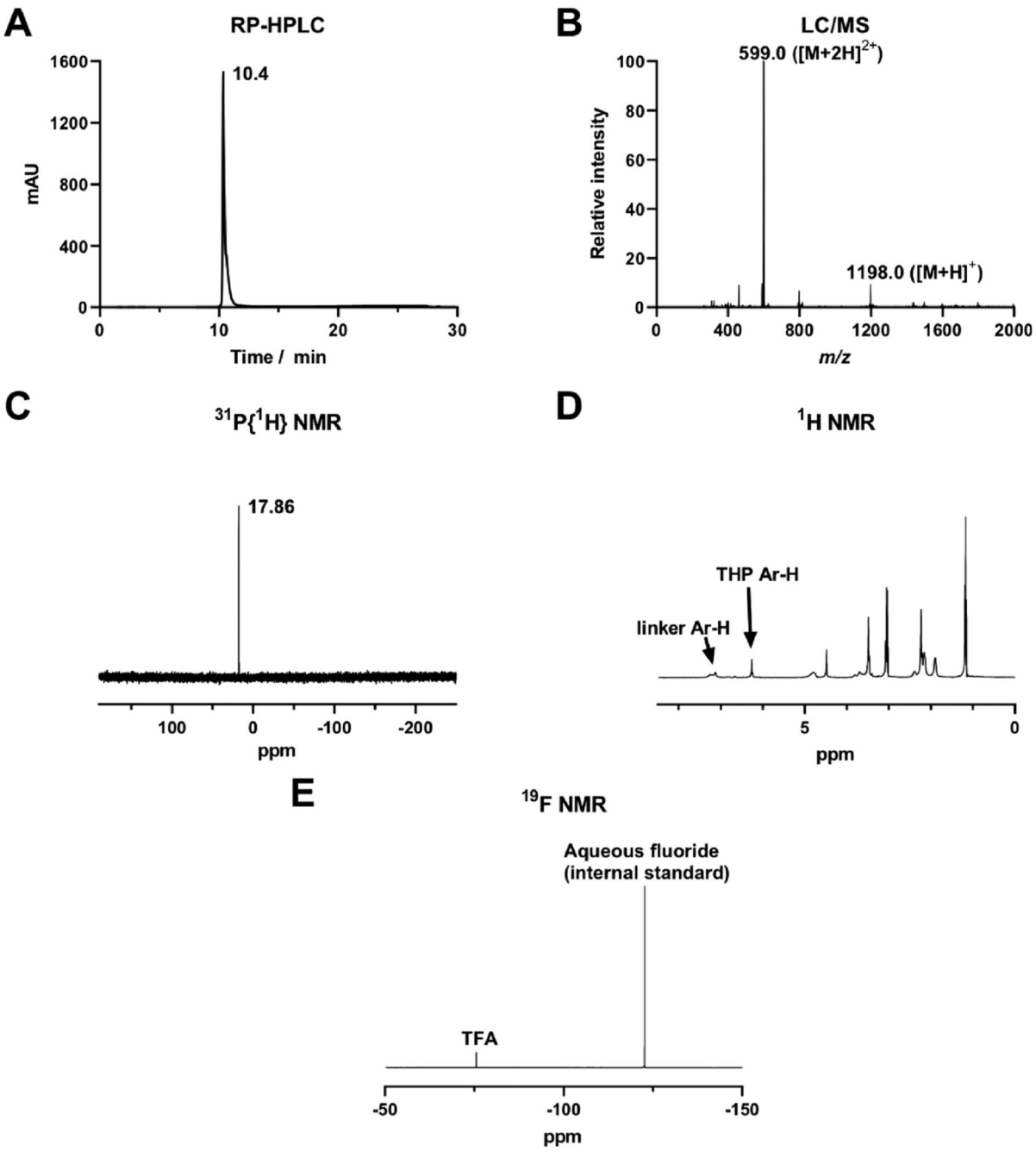

Figure 2. Characterization of THP-Pam: (A) Reverse-phase C_{18} HPLC UV (254 nm); (B) ESI-MS spectrum (+ve mode) from LC/MS; (C) $^{31}P\{^{1}H\}$ NMR in D_2O; (D) ^{1}H NMR in D_2O; (E) ^{19}F NMR in D_2O confirming the presence of TFA salts.

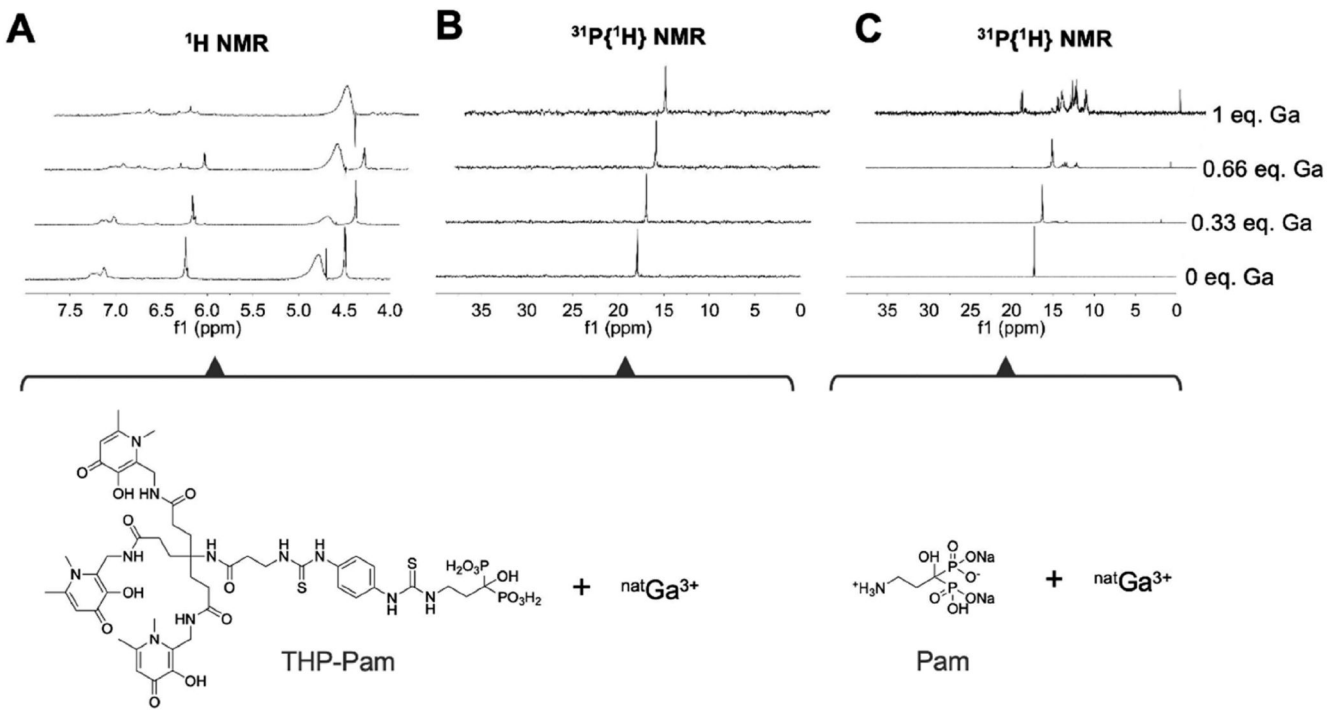

Figure 3. NMR titration experiments (D_2O and pH 9) of THP-Pam and pamidronate upon [^{nat}Ga]gallium nitrate addition demonstrating the lack of involvement of the bisphosphonate of THP-Pam in gallium binding.

Each spectrum is scaled according to the largest peak shown for the sake of clarity.(A) ^{1}H NMR 4.0-7.8 ppm window showing aromatic protons of THP-Pam corresponding to hydroxypyridinone arms, which show changes in chemical shift and loss of symmetry upon gallium binding, indicating a change in chemical environment; (B) ^{31}P{^{1}H} NMR showing that BP phosphorus atoms exhibit no chemical shift or loss of symmetry or homogeneity upon gallium binding, consistent with lack of involvement; (C) ^{31}P{^{1}H} NMR showing pamidronate binding to gallium for comparative purposes, which shows a clear loss of symmetry and homogeneity upon gallium binding.

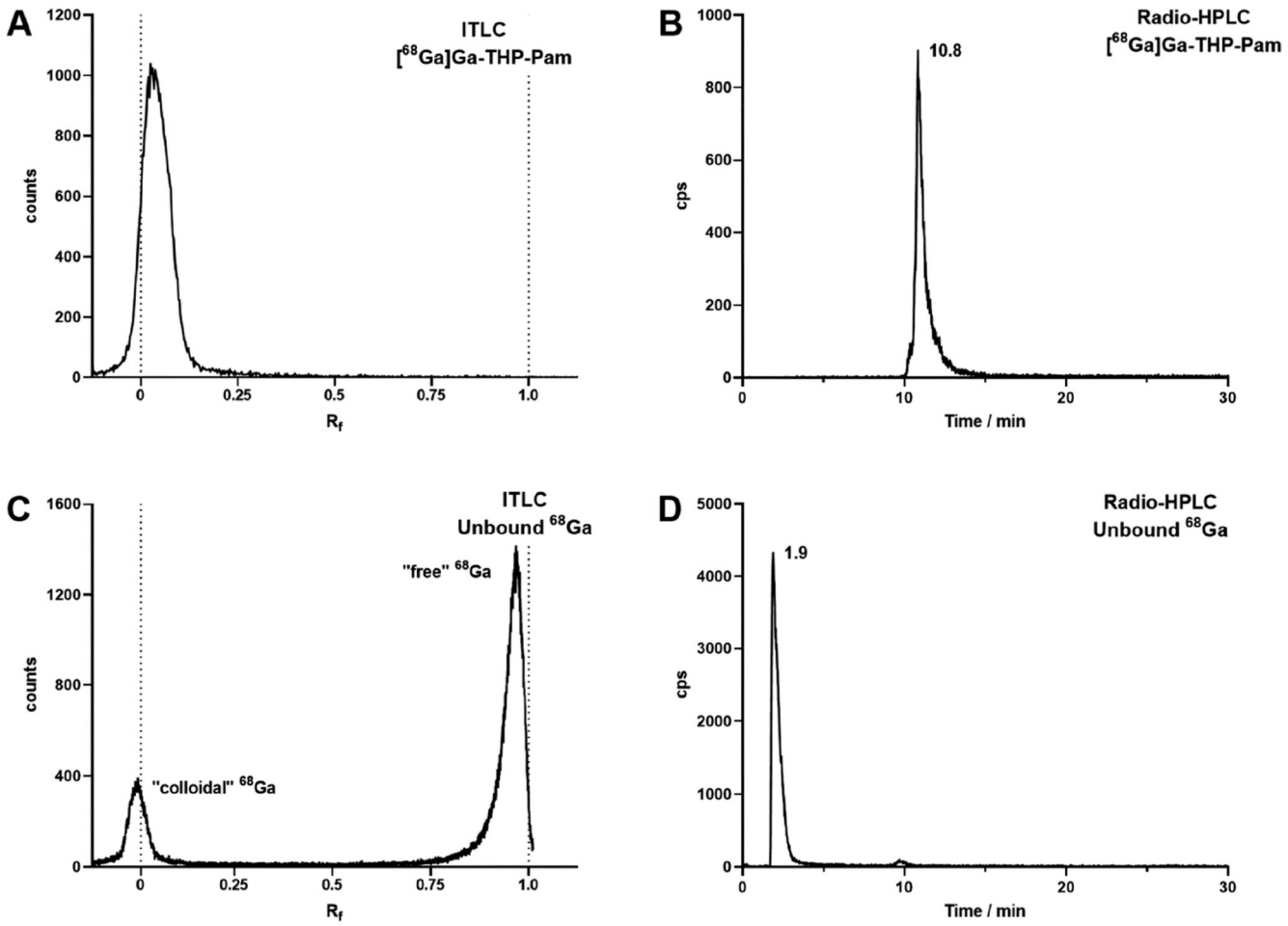

Figure 4. Radioanalysis of [^{68}Ga]Ga-THP-Pam and unbound ^{68}Ga as a comparison.

(A) ITLC of [^{68}Ga]Ga-THP-Pam in 0.5 M citrate buffer pH 5.5. (B) Reverse-phase C_{18} radio-HPLC of [^{68}Ga]Ga-THP-Pam. (C) ITLC of unbound ^{68}Ga, showing migration to the solvent front other than colloidal ^{68}Ga. (D) Reverse-phase C_{18} radio-HPLC of unchelated ^{68}Ga.

Europe PMC Funders Author Manuscripts

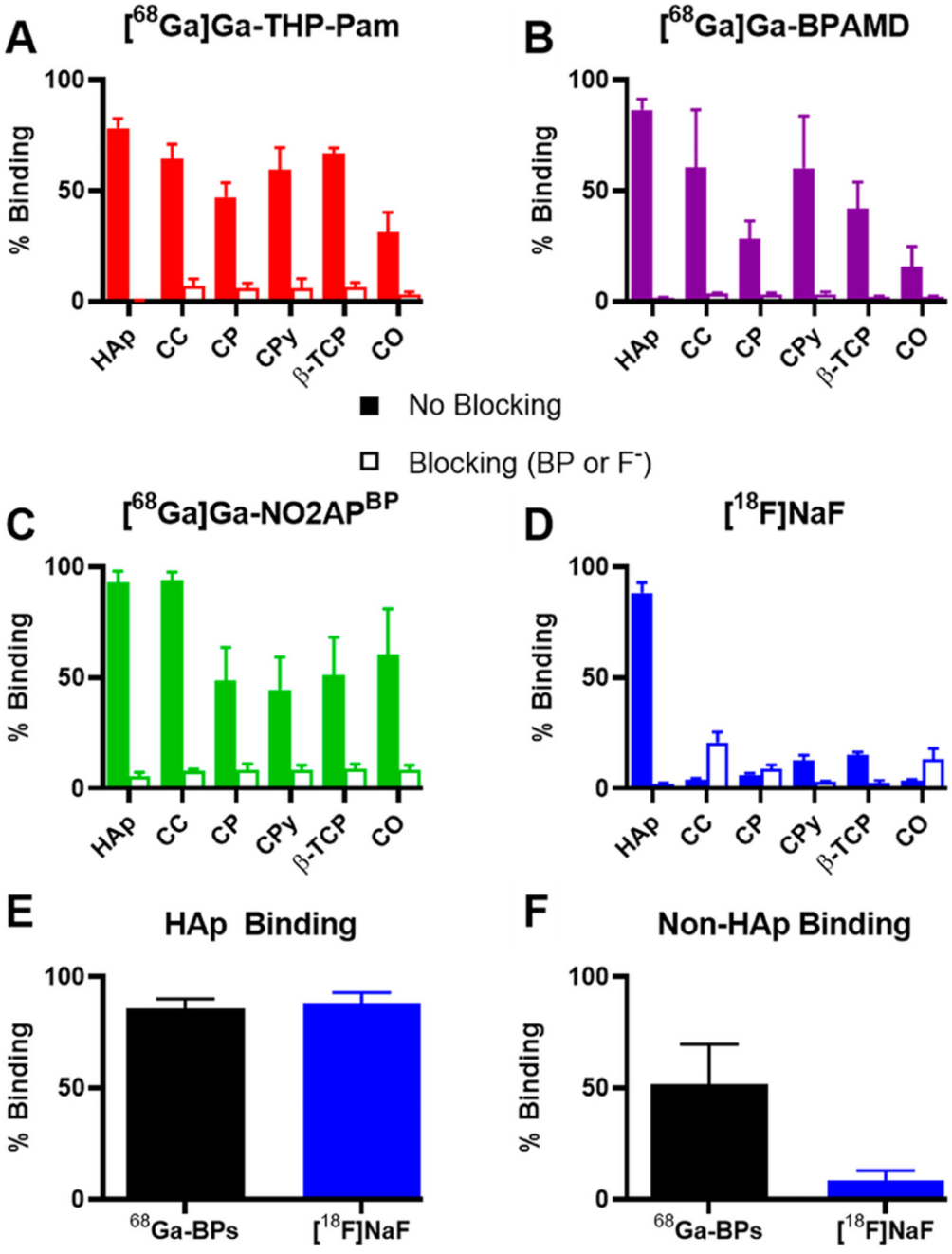

Figure 5. Binding of each radiotracer to an array of calcium salts in saline and at room temperature.

(A) [^{68}Ga]Ga-THP-Pam binding, blocking with pamidronate. (B) [^{68}Ga]Ga-BPAMD binding, blocking with alendronate. (C) [^{68}Ga]Ga-NO2AP^{BP} binding, blocking with pamidronate. (D) [^{18}F]NaF binding, blocking with sodium fluoride. (E) Comparison of the mean binding to HAp of ^{68}Ga-BPs and [^{18}F]NaF. (F) Comparison of the mean binding to non-HAp calcium salts of ^{68}Ga-BPs and [^{18}F]NaF. HAp = hydroxyapatite; CC = calcium carbonate; CP = calcium phosphate dibasic; CPy = calcium pyrophosphate; β-TCP = β-tricalcium phosphate; CO = calcium oxalate monohydrate.

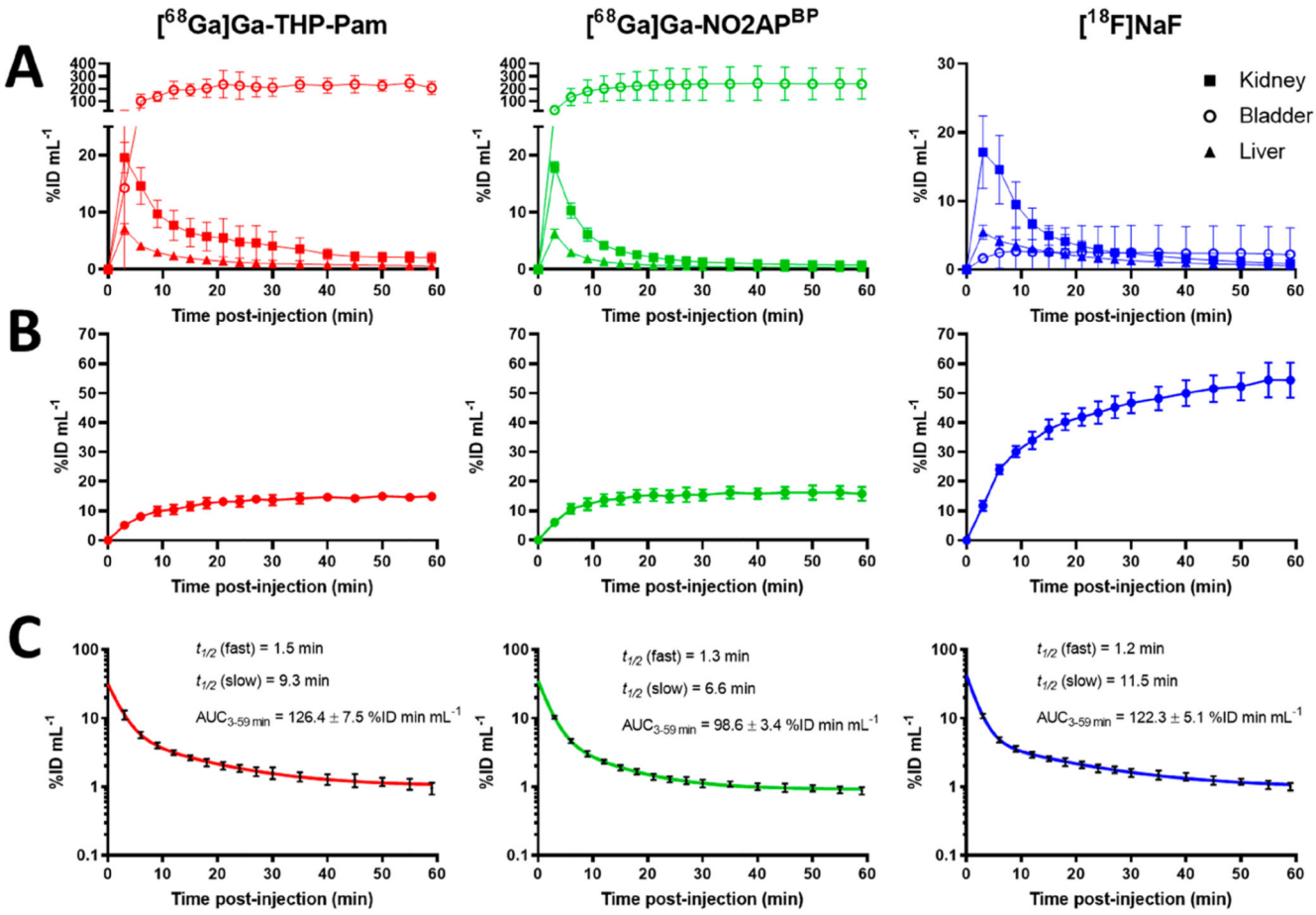

Figure 6. Pharmacokinetic data for the three PET tracers evaluated in vivo (n = 4 for each tracer).

(A) Activity (%ID/mL) over time (min) in selected organs of interest. (B) Tracer uptake in knee, used as a representative ROI of active bone. (C) Blood clearance fitted to two-compartment pharmacokinetic model using the heart as a representative ROI for blood.

Europe PMC Funders Author Manuscripts

Europe PMC Funders Author Manuscripts

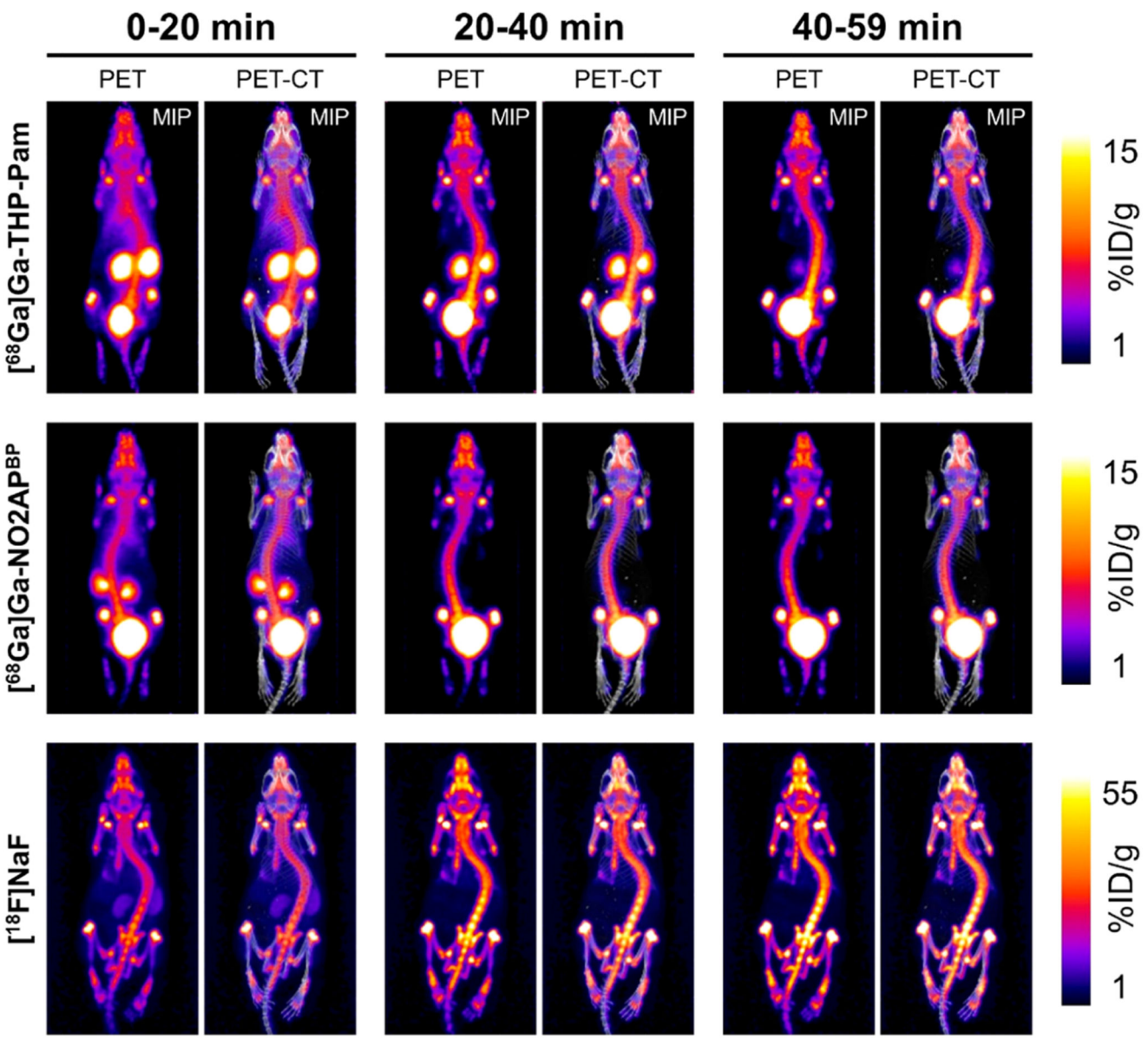

Figure 7. PET-CT study showing representative maximum intensity projection (MIP) images of each radiotracer over three windows of time in healthy BALB/c mice.

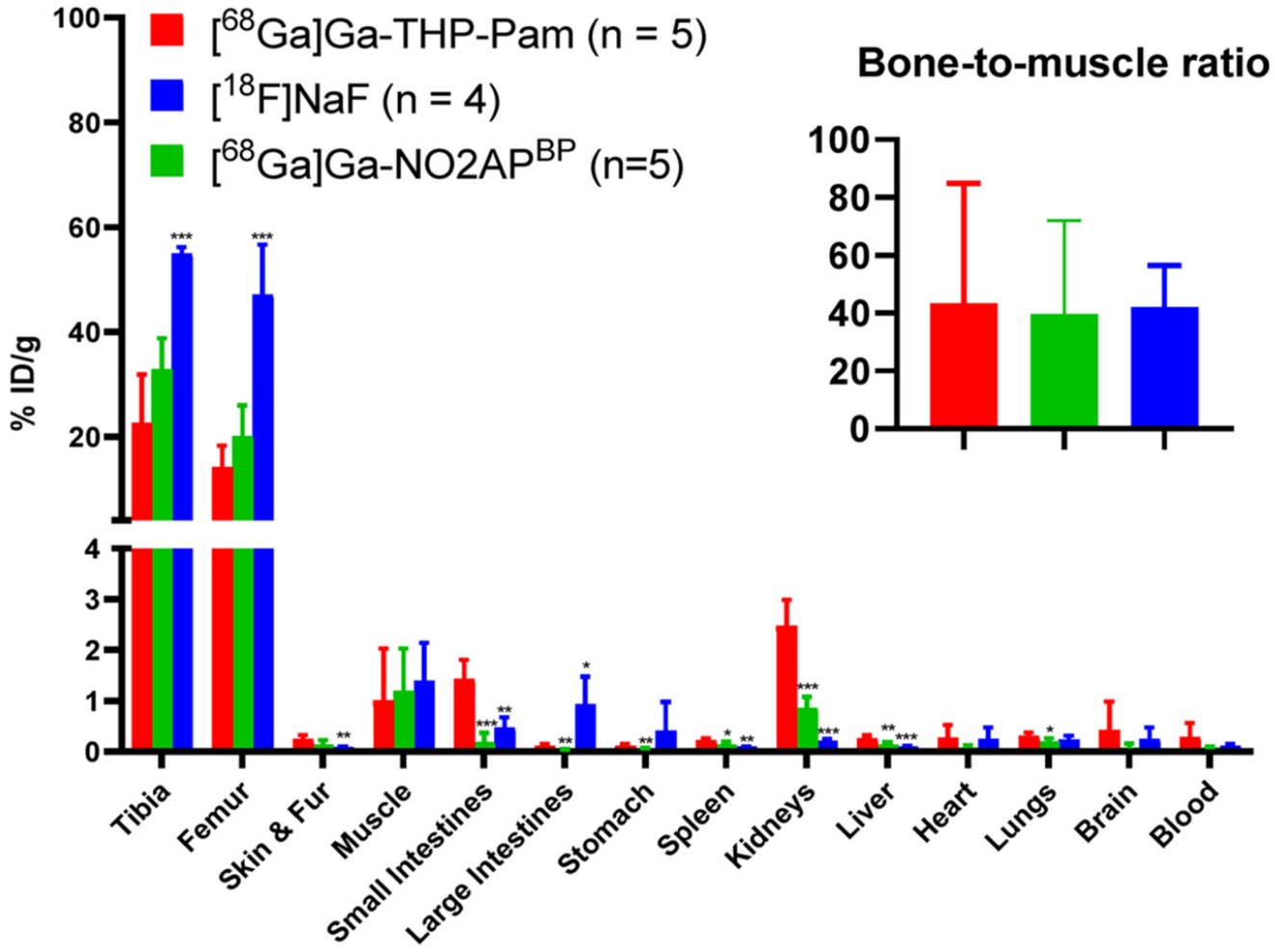

Figure 8. Ex vivo biodistribution of [^{68}Ga]Ga-THP-Pam, [^{68}Ga]Ga-NO2AP^{BP}, and [^{18}F]NaF 120 min postinjection. Bone-to-muscle ratio inset. * = p < 0.05; ** = p < 0.01; *** = p < 0.001.

Europe PMC Funders Author Manuscripts

A

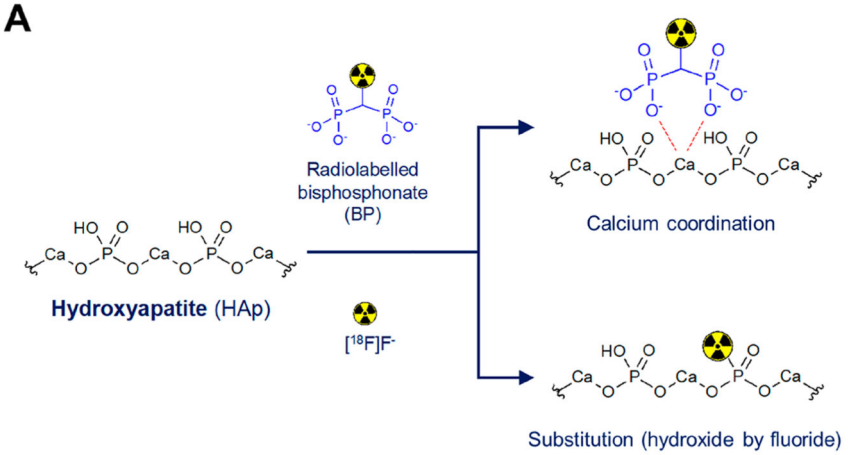

B

Calcium salt	Formula
Hydroxyapatite	$Ca_5(PO_4)_3(OH)$
Calcium oxalate	$C_2O_4Ca{\cdot}H_2O$
β-tricalcium phosphate	$Ca_3(PO_4)_2$
Whitlockite	$(Ca,Mg)_3(PO_4)_2$
Calcium carbonate	$CaCO_3$
Calcium pyrophosphate	$Ca_2P_2O_7$
Amorphous calcium phosphate	$Ca_3(PO_4)_2{\cdot}xH_2O$

Scheme 1. (A) Schematic Showing the Proposed Binding of Bisphosphonate (BP)-Based Imaging Agents and [^{18}F]NaF to Hydroxyapatite (HAp); (B) Formulae of the Different Calcium Salts Discussed in This Work

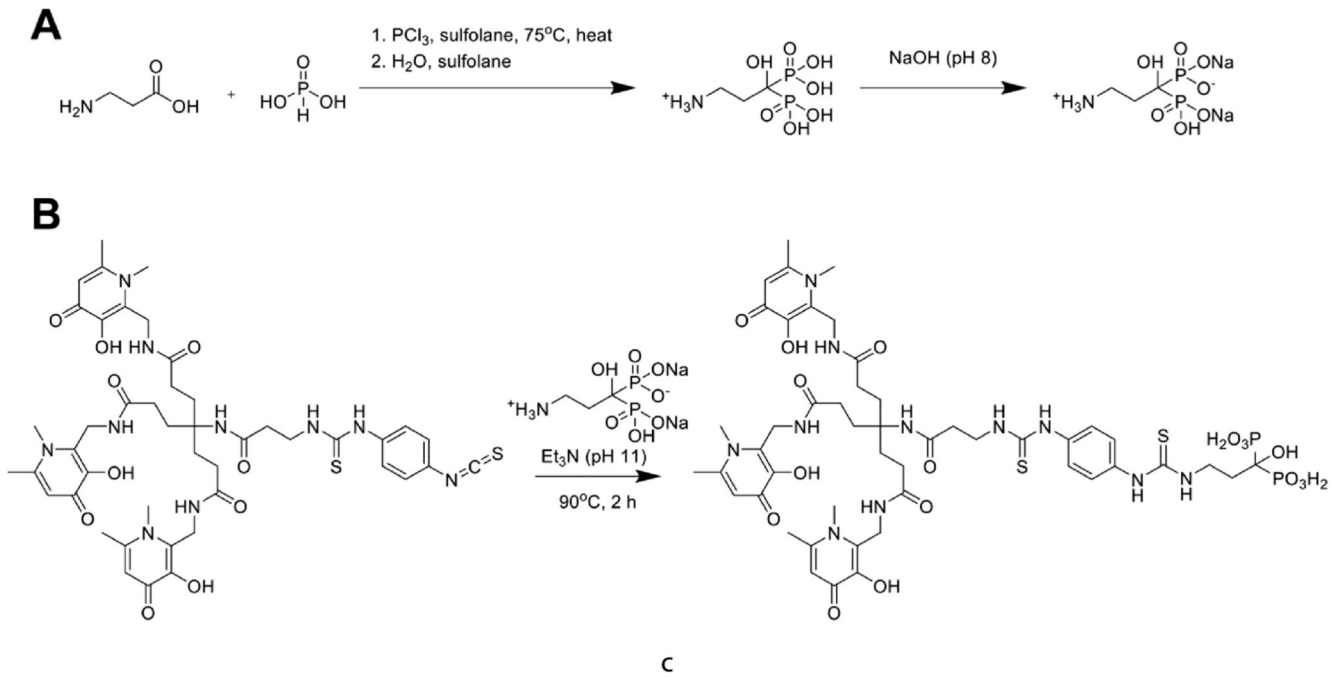

Scheme 2. Synthesis of THP-Pam: (A) Synthesis of the Amino-BP Pamidronate; (B) Thiourea Bond Formation between Pamidronate and THP-NCS Yields THP-Pam in 71% Yield

Europe PMC Funders Author Manuscripts

Europe PMC Funders Author Manuscripts

Table 1
Radiolabeling of the Tracers Evaluated in This Study

Radiotracer	Radiolabeling conditions	Other processing for *in vivo* use
[^{68}Ga]Ga-THP-Pam	Radionuclide: ^{68}Ge/^{68}Ga generator	- None.
	Reaction conditions: 5 min, room temperature, pH 7	
[^{68}Ga]Ga-BPAMD	Radionuclide: ^{68}Ge/^{68}Ga generator	- Postprocessing of ^{68}Ge/^{68}Ga generator eluate prior to radiolabeling. *
	Reaction conditions: 15 min, 95 °C, pH 4	- Cooling.
		- Cation exchange column.
		- Neutralization of reaction.
[^{68}Ga]Ga-NO2AP^{BP}	Radionuclide: ^{68}Ge/^{68}Ga generator	- Postprocessing of ^{68}Ge/^{68}Ga generator eluate prior to radiolabeling. *
	Reaction conditions: 10 min, 95 °C, pH 4	- Cooling.
		- Neutralization of reaction.
[^{18}F]NaF	Cyclotron production	- 2 ion exchange columns.

* Not essential; allows milder radiolabeling conditions and high molar activities.